Dissociative recombination of CH^+ : A calculation using the R-Matrix method

Dermot Madden

Department of Physics and Astronomy
University College London

Thesis submitted for M.Phil.
September 2012

DECLARATION BY CANDIDATE

I hereby declare that this thesis is my own work and effort and that it has not been submitted anywhere for any award. Where other sources of information have been used, they have been acknowledged.

Date:

Signature:

Abstract

CH^+ is one of many molecules important in astrophysics observations and is of interest for the formation of large hydrocarbons. A key feature of work on CH^+ has being its observed overabundance in the interstellar medium compared to calculated predictions.

The molecular R-Matrix with Pseudo-States (RMPS) method is applied to CH^+ for internuclear separations of 0.7-3.2 Angstrom using the UK Polyatomic R-Matrix codes. These calculations show the potential energy curves for the four lowest states and we identify resonances below the $^3\Pi$ threshold. We perform an initial calculation of the dissociative recombination cross sections from the resonance curves.

We also detail our contributions to the UKRmol initiative, involving the creation of a consistent core of R-matrix codes.

Contents

Acknowledgements

This thesis is dedicated to Katherine whose love and support helped me every step of the way.

Chapter 1

Introduction

1.1 CH^+

CH^+ was first identified in diffuse interstellar clouds by Douglas and Herzberg in 1941 [19]. Bates and Spitzer in 1951 [7] discussed the formation and destruction of CH^+, for destruction mechanisms they considered photodissociation, photoionzation and recombination of CH^+ with electrons:

dielectronic recombination: $CH^+ + e^- \rightarrow CH + hv$
and dissociative recombination: $CH^+ + e^- \rightarrow C + H$

They noted that the dissociative recombination might be rapid but because of uncertainties in many reaction rates, it was difficult to match abundances with observations [18]. It was 21 years before Bates and Spitzer's work was improved on by Soloman and Klemperer in 1972 [61], however one of their critical assumptions was that the relative rates of dielectronic recombination and dissociative recombination were equal. They assumed those rates were $\approx 10^{-10} cm^3 s^{-1}$, however dissociative recombination is generally quite fast with typical rates of $\approx 10^{-7} cm^3 s^{-1}$ [30]. The prerequisite for rapid dissociative recombination is a dissociative potential curve of the neutral within the

Franck-Condon region of the ion. However Solomon and Klemperer argued that the observed abundance of CH^+ in interstellar clouds indicated that the dissociative recombination rate could not be of the rapid variety.

A number of theoretical studies looked at the CH^+ dissociative recombination rate. Bardsley and Junker [5] and also Krauss and Julienne [36] concluded that an appropriate neutral state crossed the CH^+ Franck-Condon region, suggesting a fast dissociation rate. However Giusti-Suzor and Lefebvre-Brion [26] noted that expanding the calculations to include Rydberg states could displace the potential curves and produce a slower dissociation rate. Subsequent experiments by Michell and McGowan [40] suggested that the rate is indeed fast $\approx 10^{-7} cm^3 s^{-1}$, however it is possible that the fast measured rate may apply only to vibrationally excited CH^+ while that in interstellar space is all in $v = 0$. Rapid destruction of CH^+ by dissociative recombination makes it difficult to produce enough CH^+ to match observed abundances.

There have been a number of recent theoretical [65] and experimental [2, 45, 24] studies of this problem. However there remains issues with the accurate prediction of the rate of dissociative recombination under astrophysical conditions as the accurate prediction of excited state curve crossings is difficult.

1.2 R-Matrix with Pseudostates (RMPS) method

The R-matrix method provides a rigorous *ab initio* procedure for studying electron molecule collisions and, in the context of dissociative recombination, for providing resonance curves and widths ("couplings").

The R-Matrix approach is based on dividing configuration space into two regions. The inner region is defined by a sphere of radius a, centred at the centre-of-mass of the molecule. This sphere is chosen to enclose the target

charge distribution. In the inner region the interactions are strong and multi-centred and include both exchange and correlation between the scattered electron and the electrons of the target. In the outer region, exchange and correlation effects are neglected as only the long range multi-pole potential is important. For electron-CH^+ scattering, the long-range Coulomb forces are accounted for by the use of Coulomb functions in the asymptotic region; the main issue is therefore to account for the effects of the target dipole moment at long-range.

The R-matrix method, in common with other close-coupling methods, only includes a finite number of states in the close-coupling expansion. It therefore, of necessity, does not account for higher-lying target states or the target continuum. Intermediate energy processes, where the collision energy lies near to or above the ionisation threshold, cannot be treated correctly without accounting for these states. The RMPS method which was developed by Bartschat et al 1996[6] for atoms and implemented by Gorfinkiel and Tennyson [29, 72] for molecules, includes an extra pseudo-continuum basis set which allows for the construction of an extra set of target states. These are referred to as pseudostates as they are not true eigenstates of the target molecule, but they can, if selected correctly, be used to describe the missing electronic target states and the continuum which is discretized within the R-matrix sphere. The method also gives a significant improvement to the treatment of target polarisation [35].

1.3 Objectives

The objective of this project is to apply the R-matrix with Pseudostates method to CH^+ and determine if it can better reproduce target polarisation and if so go on to use the method to generate accurate energy curves and resonances which will be used to calculate the dissociative recombination rate coefficient using multi-channel Quantum Defect Theory.

In order to perform these calculations we contributed to the UKRmol initiative, helping to produce a consistent working set of R-matrix codes.

Chapters 2, 3 and 4 will cover background theory, the R-Matrix theory and give an overview of the UKRmol implementation that was used for these calculations, along with details of our contributions to the UKRmol project[1]. Chapters 5 and 6 will cover the CH^+ model chosen for the calculation and the results achieved.

Chapter 2

Theory Background

2.1 Introduction

This chapter gives a brief overview of dissociative recombination and the approximation methods used in order to solve the electron-molecule scattering problem.

2.2 Dissociative Recombination

For a diatomic molecular ion, dissociative recombination is a collision process through one of the following two reaction paths:

$e + AB^+ \rightarrow \qquad AB^{**} \rightarrow A + B$

$e + AB^+ \rightarrow AB^* \rightarrow AB^{**} \rightarrow A + B$

Both paths involve the formation of a doubly excited AB^{**} dissociative state of the neutral molecule, sometimes referred to as the resonant state. This resonant state yields the atomic products A and B. In the first pathway the electron+ion continuum is directly coupled to the repulsive state AB^{**}. The second pathway proceeds through an intermediate step, corresponding to electron capture in the Rydberg level AB^*. Which is associated with a

vibrationally excited state of the initial ion AB^+. These two reaction paths are shown in Figure 2.1 and are called the direct and indirect processes.

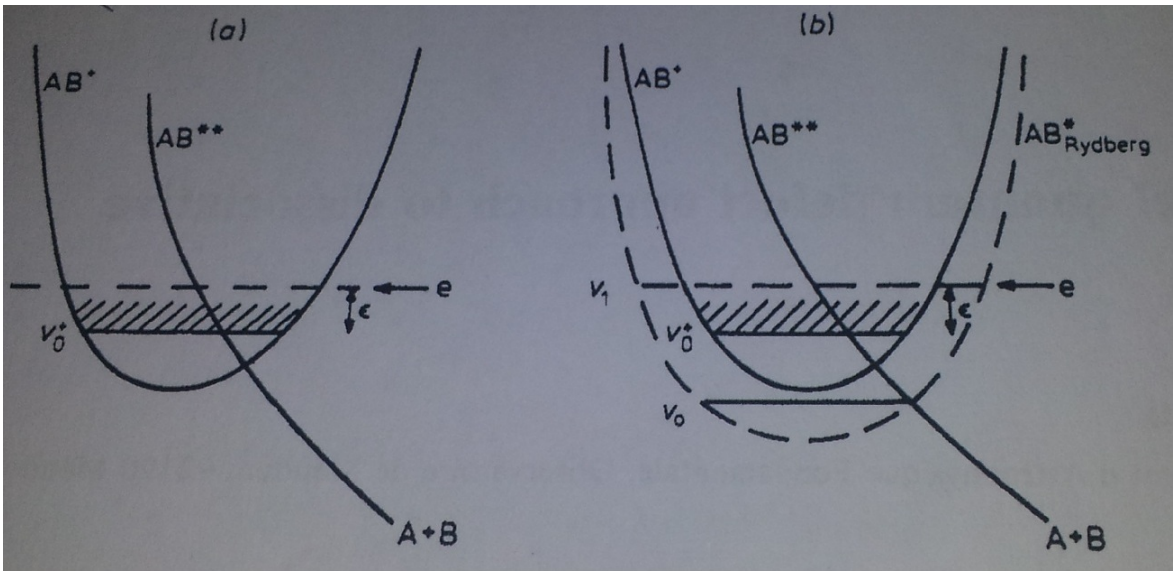

Figure 2.1: Dissociative recombination of a diatomic molecular ion; (a) direct process (electronic capture in the dissociative state AB^{**}), (b) indirect process via vibrational capture in a Rydberg state AB^* predissociated by AB^{**}. (Giusti 1980 [27]).

2.3 Born-Oppenheimer Approximation

The molecular Hamiltonian for N_e electrons and N_n nuclei in the non-relativistic time-independent Schrodinger equation can be written in atomic units as

EQ2.1:

$$H = -\frac{1}{2}\sum_{i=1}^{Ne} \nabla_i^2 - \sum_{A=1}^{Nn} \frac{1}{2M_A} \nabla_A^2 - \sum_{A=1}^{Nn}\sum_{i=1}^{Ne} \frac{Z_A}{|r_i - R_A|} + \sum_{j=1}^{Ne}\sum_{i>j}^{Ne} \frac{1}{r_i - r_j} + \sum_{A=1}^{Nn}\sum_{B>A}^{Nn} \frac{Z_A Z_B}{|R_A - R_B|}$$

The first and second terms are the kinetic energies of the electrons and the

nuclei. The third term is the attractive electron-nucleus Coulomb potential. The final two terms represent the repulsive electron-electron and nuclear-nuclear potentials.

The Born-Oppenheimer approximation is based on the property that the electrons in the molecule are much lighter than the nuclei and so move more much more rapidly. The approximation assumes that the electrons around the nuclei can respond instantaneously to even a small motion of the nuclei and so the nuclei can be assumed to be fixed. With this assumption the second term (the kinetic energy of the nuclei) in equation 2.1 can be neglected and the last term (the nuclear-nuclear repulsion) can be regarded as a constant. The remaining Hamiltonian describes the motion of N electrons in the field of N_n point charges and can be written as

EQ2.2:

$$H_{elec} = -\frac{1}{2}\sum_{i=1}^{Ne} \bigtriangledown_i^2 - \sum_{A=1}^{Nn}\sum_{i=1}^{Ne} \frac{Z_A}{|r_i - R_A|} + \sum_{j=1}^{Ne}\sum_{i>j}^{Ne} \frac{1}{r_i - r_j}$$

The time-independent Schrodinger equation may be written as

EQ2.3:

$$H_{elec}\psi_{elec}(r_i; R_A) = \varepsilon_{elec}\psi_{elec}(r_i; R_A)$$

Its solutions depend explicitly on the electronic coordinates r_j and parametrically on the nuclear coordinates, R_A. That means that for any arrangement of the nuclei, the electronic wave function ψ_{elec} is a different function of the electronic coordinates.

The total energy for fixed nuclei includes the constant repulsion of the nuclei:

EQ2.4:

$$E_{elec} = \varepsilon_{elec} + \sum_{A=1}^{Nn}\sum_{B>A}^{Nn} \frac{Z_A Z_B}{|R_A - R_B|}$$

This energy is known as the electronic potential. The nuclear motion can be solved under the same assumptions as the electronic part of the problem. As the electronic motion is much faster than the nuclear motion, the electronic

motions of equation 2.1 can be replaced by the average values. The Hamiltonian for the motion of the nuclei in the average field of the electron can be written as:

EQ2.5:

$$H_{nucl} = -\sum_{A=1}^{N_n} \frac{1}{2M_A} \nabla_A^2 + E_{elec}(R_A)$$

The total energy $E_{elec}(R_A)$, gives a potential for nuclear motion. This function gives a potential energy surface as a function of nuclear geometries, R_A. In the Born-Oppenheimer approximation the nuclei move on a potential energy surface produced by solving the electronic problem.

2.4 Hartree-Fock Self Consistent Field Method

The Born-Oppenheimer approximation equation 2.2 can not be solved exactly. The first step to a solution is to use the Hartree-Fock (HF) approximation. This treats the motion of each electron in the attractive field of the nuclei and the averaged field of the remaining (N-1) electrons. Each electron is described by a spin-orbital which is a wave function defining the spatial distribution of an electron and its spin. From the variational principle, the simplest wave function for a closed shell, N-electron molecular or atomic system can be described by a Slater determinant [64], with the condition that the spin-orbitals ξ_i remain orthonormal.

EQ2.6:

$$|\Psi> = |\chi_1 \chi_2 \cdots \chi_a \chi_b \cdots \chi_N>$$

The best wave function gives the lowest value of electronic Energy E_0, the spin-orbitals are modified by minimising E_0. The HF eigenvalue equation can be written as

EQ2.7:

$$\hat{f}(1)\chi_a(1) = \varepsilon_a \chi_a(1)$$

where ϵ_a is the orbital energy of χ_a. Operator $\hat{f}$ is defined as the Fock

operator and contains the core-Hamiltonian operator $\hat{h}$ and the one-electron potential operator G.

EQ2.8:

$$\hat{h}(1) = -\frac{1}{2} \bigtriangledown_1^2 - \sum_{A=1}^{Nn} \frac{Z_A}{r_{1A}}$$

EQ2.9:

$$\hat{f}(1) = \hat{h}(1) + G(1)$$

G is the Hartree-Fock potential and can be written as

EQ2.10:

$$G(1) = \sum_{b \neq a} [\jmath_b(1) - \kappa_b(1)]$$

where $\jmath$ is the Coulomb operator and represents the Coulombic repulsion between electrons (1) and (2) and κ is the exchange operator which represents the effect of the Pauli principle

The Hartree-Fock approximation simplifies the many electron problem to an effective one electron problem by treating the electron-electron repulsion in an averaged way. The HF equation is solved iteratively using the self-consistent field (SCF) approach. This works by estimating and initial set of spin-orbitals, obtaining the one electron HF potential and solving the HF equation to get a new set of spin-orbitals. This process is then repeated with the new set of spin-orbitals until self-consistency is reached. From this process we get two types of spin-orbitals: occupied, the N spin-orbitals with the lowest energies and virtual, which lie at higher energies and are not occupied.

2.5 Configuration Interaction

The HF approximation does not give an exact solution of the non-relativistic time-independent electronic Schrodinger equation. Its limitations arise as the motions of electrons with opposite spin are not correlated. The difference between the exact non-relativistic energy of the system and the HF energy is known as the correlation energy.

EQ2.11

$$E_0 = E_{corr} + E_{HF}$$

The correlation energy can be calculated using the configuration interaction (CI) method. The method is to diagonalise the N-electron Hamiltonian in a basis of N-electron functions. In other words, the correlation can be calculated by the variational method with the exact wave function as a linear combination of either configuration state functions (CFSs) or Slater determinants.

If N-tuply excited configurations are included, the CI expansion for an N-electron wave function is complete, and is called a Full CI (FCI) and produces a complete solution of the non-relativistic Schrodinger equation. The size of the Hamiltonian matrix grows with the size of the basis set so full CI is only practical for small molecules.

A modification to make the calculation more practical, and used in the calculations carried out as part of this project, is to use the complete active space CI (CAS CI). In the CAS CI the orbitals are divided into core, virtual and active. The lowest energy core orbitals are doubly occupied in all CSFs, the higher energy virtual orbitals are unoccupied and the medium energy active orbitals vary in occupancy [60]. The CAS CI does a FCI expansion within the chosen active orbitals.

2.6 Fixed-nuclei Formation/Scattering

In considering electron-molecule collisions it is important to distinguish between electronic and nuclear coordinates within the molecule. Two reference frames [37] can be used to simplify the equations describing the collision process. The BODY (Fig 2.2) frame has a system of coordinates fixed with respect to the molecule and the body fixed z axis is along the maximum symmetry axis of the molecule. The LAB frame (Fig 2.3) has the z axis fixed along the initial momentum vector of the incident particle. The common origin point for both systems is the centre of mass of the molecule. r and R are the position vectors of the electrons and the nuclei of the molecule, respectively and r_p is the coordinate of the scattering particle in the BODY frame. Primed coordinates signify the LAB frame.

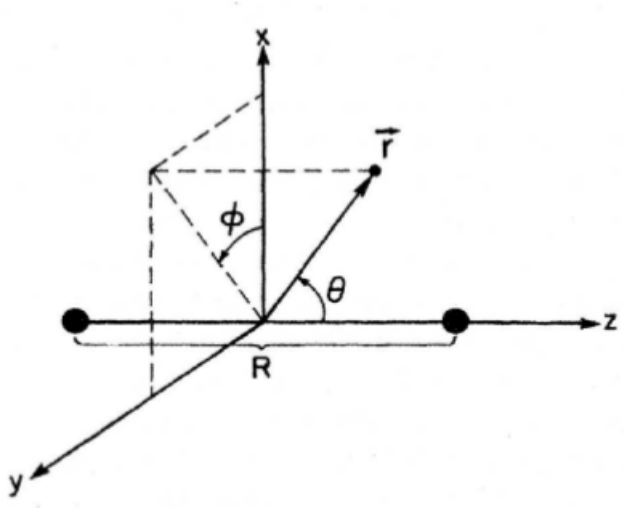

Figure 2.2: Electronic coordinates of a molecular system in the BODY frame. (Lane 1980)

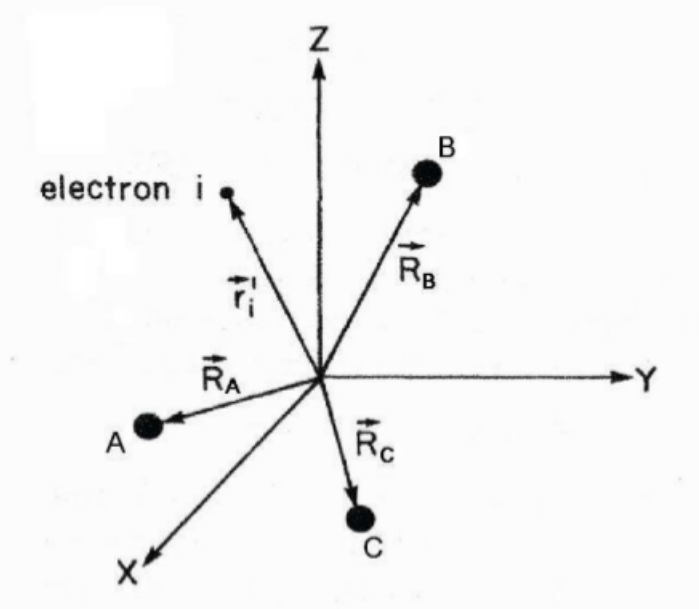

Figure 2.3: Coordinates of a molecular system in LAB frame: e_i is the electron. A,B and C are the nuclei. (Lane 1980).

The Hamiltonian for the particle-molecule collision can be written as

EQ2.12:

$$H_{N+1} = -\frac{1}{2} \bigtriangledown_{\gamma}^{2} + H_{N}^{elec} + V_{p-m}$$

where $\bigtriangledown_{\gamma}^{2}$ is the Laplacian of the scattering particle in the BODY frame. H_{N}^{elec} is the N-electron target Hamiltonian given by equation 2.2 and V_{p-m} is the positive charged particle-target molecule interaction potential energy.

For a target molecule the electronic states are represented by functions $\psi_{A}^{elec}(r, R)$, where A is the electronic quantum number. These wave functions must satisfy the electronic Schrodinger equation (EQ2.3). For fixed-nuclei approximation the Schrodinger equation for $N_e + 1$ system is

EQ2.13:

$$(H_{N+1} - \varepsilon)\Psi_{\varepsilon}^{F}{}_{N}(r_p, r; R) = 0$$

This approximation is accurate in the region where electrons are close to the nuclei and their motion can be considered dominant in the interaction potential energy.

Chapter 3

R-Matrix Theory

The R-matrix method, in common with other close-coupling methods, only includes a finite number of states in the close-coupling expansion. It therefore, of necessity, does not account for higher-lying target states or the target continuum. Intermediate energy processes, where the collision energy lies near to or above the ionisation threshold, cannot be treated correctly without accounting for these states. The R-matrix with Pseudo-States (RMPS) method includes an extra pseudo-continuum basis set which allows for the construction of an extra set of target states. These are referred to as pseudostates as they are not true eigenstates of the target molecule, but they can, if selected correctly, be used to describe the missing electronic target states and the continuum which is discretized within the R-matrix sphere.

The previous R-matrix study of resonance curves in the CH^+ system used Slater Type Orbitals (STOs) to represent the target and numerical functions for the continuum [69]. Since the RMPS method is only implemented in the polyatomic R-matrix code [43], both target, continuum and, indeed, pseudo-continuum orbitals are represented using Gaussian Type Orbitals (GTOs). For continuum orbitals GTOs up to and including g waves were used [21]. The polyatomic R-matrix code cannot treat linear symmetries and all calculations were performed in C_{2v} symmetry. It is reasonably straightforward

to reconstruct the full symmetry from these calculations particularly since considerable care was taken to ensure that the calculation preserved the degeneracy structure of the calculations.

A comprehensive review of molecular R-matrix calculations [72] has recently being published and is best placed to provide detailed explanations of the method. A brief overview will be given here.

3.1 Overview of R-Matrix

R-Matrix was originally applied to the study of nuclear collisions by Wigner in 1946[73] and Wigner and Eisenbud in 1947[74]. The first application of R-Matrix techniques to atomic scattering by electrons came in the 1970s (Burke et al 1971 [12], Burke and Robb 1975[9], Burke 1976[10]). Schneider in 1975[57] and Schneider and Hay in 1976[58] and Burke et al in 1977[11] applied R-Matrix theory to electron-molecule scattering. This was followed by developments studying electron collisions with diatomic molecules and expanded by Nestmann et al in 1994[47] to polyatomic molecules.

EQ3.1:

$$H_{N+1}\Psi = E\Psi$$

The R-Matrix approach is based on dividing configuration space into two regions. The inner region is defined by a sphere of radius a, centred at the centre-of-mass of the molecule. This sphere is chosen to enclose the target charge distribution. In the inner region the interactions are strong and multi-centred and include both exchange and correlation between the scattered electron and the electrons of the target. In the outer region, exchange and correlation effects are neglected as only the long range multi-pole potential is important.

In the inner region, a close-coupling expansion is used to calculate a series of energy independent eigenfunctions and eigenvalues for the N+1 electron system. In the outer region, the R-Matrix constructed on the boundary

is propagated outwards [41], until the solutions to the inner region can be matched with asymptotic solutions. Asymptotic expansion methods are used to get the K-Matrix and from that eigenphase sums and T-matrix can be calculated. The T-matrix is in turn used for scattering information such as cross sections.

For electron-CH^+ scattering, the long-range Coulomb forces are accounted for by the use of Coulomb functions in the asymptotic region; the main issue is therefore to account for the effects of the target dipole moment at long-range.

3.2 Inner Region

The target molecule wave function is described by a set of basis functions representing the molecular orbitals as a linear combination of atomic orbitals centred on the nuclei. These orbitals describe the molecular charge distribution which must be small at the R-matrix surface. The UK R-Matrix implementation uses Gaussian type orbitals (GTOs)to represent polyatomic molecules.

The scattered electron is described by a set of continuum orbitals centred on the centre of gravity of the molecule. They have a longer range then the orbitals centred on the nuclei and do not vanish on the R-matrix boundary. The Gaussian continuum basic functions are found using the method of Faure et al 2002[21], which constructs the GTO continuum basis sets for representing both Bessel and Coulomb functions. The integrals are performed over the whole configuration space and the contribution from the outer region, outside the R-matrix sphere is subtracted from the integrals over an infinite range [42]. Schmidt orthogonalisation is used to orthogonalise the continuum molecular orbitals to the target orbitals. The continuum molecular orbitals are then orthogonalised among themselves and linearly dependent functions removed [47][42].

The inner region scattering energy independent eigenfunctions of the (N+1)-electron system can be represented by

EQ3.2:

$$\psi_k^{n+1} = A \sum_I \psi_I^N(X_1, ..., X_N) \sum_j \bar{\xi}_j(X_{n+1}) a_{Ik} + \sum_m \chi_m(X_1, ..., X_N, X_{N+1}) b_{mk}$$

where A is the anti-symmetrisation operator, $X_n = (r_n, \sigma_n)$ for which r_n is the spatial coordinate and on the spin state of the n^{th} electron, $\bar{\xi}_j$ is a continuum molecular orbital spin couple with the scattered electron and a_{ijk} and b_{mk} are variational coefficients. The first summation term runs over the target states. It represents one electron in a continuum state with remaining electrons in a target state, known as a 'target plus continuum' configuration. The second summation term runs over configurations χ_m in which all the electrons occupy target molecular orbitals and are known as L^2 functions. These configurations account for correlation effects such as virtual excitation to higher electronic states. To make the Hamiltonian matrix Hermitian inside the R-Matrix sphere, the Bloch operator [8] is included. The variational coefficients a_{ijk} and b_{mk} are obtained when the Born-Oppenheimer Hamiltonian matrix is diagonalised. The matrix elements are determined as the individual target configurations and are reconstructed to ones written as the CI target wave functions. The size of the transformed Hamiltonian matrix is significantly reduced in a process called CI contractions[71] as the number of target states is usually smaller than the number of terms in the CI expansion. The R-matrix on the boundary can be defined from the solutions to the Hamiltonian matrix. The R-matrix gives a complete description of the scattering problem in the inner region and gives the necessary boundary conditions to match the outer and inner region wave functions.

3.3 Outer Region

The R-matrix is propagated to a radius [41] where the interaction between the scattered electron and target molecule is considered to be small.

EQ3.3:

$$R_{ij}(E) = \frac{1}{2a}\sum_{k}\frac{f_{ik}(a)F_{jk}(a)}{e_k - E}$$

E is the total energy of the system and e_k are the eigenvalues of the Hamiltonian matrix. The R-matrix above is summed over the surface amplitudes f_{ik} and sub-sequentially over the eigenfunctions ψ_k^{N+1} as the surface amplitudes f_{ik} can be written as

EQ3.4:

$$f_{ik} = < \psi_{I_i}^N Y_{I_i m_{l_i}} | \psi_k^N {}_{+1} >$$

where $\psi_{I_i}^N Y_{l_i m_{l_i}}$ are channel functions.

In the outer region the exchange and detailed electron-electron correlation between the scattering electron and the target electrons are negligible. The scattering electron moves in the long-range potential of the target molecule and a single close-coupling expansion of the scattering wave function can be used.

Gailitis asymptotic expansion methods are then used to solve the outer region problem (Noble and Nesbet, 1984)[48]. In the limit case $r \to \infty$ the reduced radial functions F_i have asymptotic solutions j for each open channel i

EQ3.5:

$$F_{ij} \sim \frac{1}{\sqrt{k_i}}(sin(k_i r - \frac{1}{2}l_i\pi)\delta_{ij} + cos(k_i r - \frac{1}{2}l_i\pi)K_{ij})$$

and $F_{ij} \sim 0$ for closed channels. The coefficients K_{ij} describe the real symmetric K-matrix, which contains all the scattering information. The radial function decays exponentially in closed channels

EQ3.6:

$$F_{ij} \sim e^{-|k_i|r}$$

The eigenphases sums, δ, are obtained from the diagonalised K-matrix K^D_{ii}, which is summed over the channels.

EQ3.7:

$$\delta = \sum_i arctan(K^D_{ii})$$

The eigenphase sums are used to search for resonances, fitting them to a Breit-Wigner form.

3.4 Resonances

The cross section and eigenphase sum mainly vary slowly as a function of energy. However there are cases where the eigenphase sum increases quickly in some energy intervals of width Γ about a given energy E^r. The corresponding partial cross section changes in that energy range. This phenomenon is called a resonance. A resonance can be considered as a long lived metastable state of the target molecule in which the scattering electron is temporarily trapped. The lifetime τ of the metastable state is usually longer than the collision time.

A resonance can be described by two values: position E^r_i and width Γ^r_i. The eigenphase sum is fitted to a Breit-Wigner profile and the resonance parameters obtained:

EQ3.8:

$$\eta(E) = \sum_i tan^{-1}\left[\frac{\Gamma^r_i}{E - E^r_i}\right] + \sum_j a_j(E)E^j$$

where $a_j(E)$ is the background eigenphase and the $\eta(E)$ is the eigenphase sum. Matching resonances to the Breit-Wigner profile can be difficult if the resonance lies near a threshold, another method is to look at the time delay matrix in which resonances show up in Lorentzian form. Time delay shows

the extra time of flight of the electron due to interaction with the target. The relationship resonance width Γ and the lifetime τ can be expressed by EQ3.9: $\tau \simeq \frac{h}{2\pi\Gamma}$

Resonances can be considered as three types, shape and core-excited resonances which can be found in atoms and molecules and nuclear-excited resonances which only appear in molecules.

Shape resonances are defined as a one-electron event and happen when the scattering electron is captured by the effective potential, which is created by the target molecule, before tunnelling out. They are normally broad and have short lifetimes as they easily decay back into the ground state. Shape resonances are usually linked with the ground state of the target molecule and typically lie a few eV above the ground state.

Core-excited resonances occur when the scattering electron excites the target molecule and is captured or forms a quasi-bound state. These resonances are linked with excited states where the captured electron is in an orbital of the excited target state. core-excited resonances are classified as core-excited shape resonances or Feshbach resonances.

Feshbach resonances[22][23] are closed-channel resonances and are associated with parent single excited states which have a positive electron affinity. This resonance type lies below the parent and the resonance energy curve follows the energy curve of the parent. This means the resonance must decay into a lower state, not the parent, Feshbach resonances are typically narrow and long lived.

Core-excited shape resonances are associated with parents of negative electron affinity and lies above its parent state. So this resonance can decay into lower target states but typically prefer to decay into the parent excited state.

Nuclear excited resonances can be found at low energy, when the N+1 electron system has a weakly bound state. This resonance is typically low in energy and very narrow. The nuclear excitation is vibrational excitation

or nuclear motion, rather than excitation of the nucleus. Nuclear excited resonances always appear when the target molecule is an ion and can only be examined by going beyond the Born-Oppenheimer approximation.

3.5 RMPS

The close-coupling expansions used in the standard R-matrix method are incomplete as they do not account for the continuum of the target and can not include all excited target states. This lack of completeness leads to a significant loss of the polarisation effects for low energy collisions. The improvement in polarisabilities calculated for various molecules by including pseudostates in the calculation was shown by Jones and Tennyson 2010 [35]. The standard R-matrix approach can not treat intermediate energy processes, where the collision energy lies above or near the ionisation threshold. The R-matrix with pseudostates (RMPS) method was developed by Bartschat et al 1996 [6] and implemented as part of the UK R-matrix polyatomic code (Morgan et all 1998 [43]) by Gorfinkiel and Tennyson 2004 [28].

The core idea of the RMPS method is to include a number of wave functions Φ_i which correspond to pseudostates in the close-coupling expansion. These are not true eigenstates of the target molecule but if selected correctly they can describe the electronic continuum and also high lying target states not included in the close-coupling expansion. The pseudostates are acquired by diagonalising the target Hamiltonian matrix described in a suitable basis of configurations. A set of appropriate configurations are added in the CI expansion so that the pseudostates that are being used to represent the target continuum states are able to reproduce the electron density of the ionised system. To achieve this an extra set of orbitals, called pseudo continuum orbitals (PCOs) are introduced to obtain configurations which describe the ionised target. For the RMPS method the CI expansion changes to include two sets of configurations, the usual configuration set in which all electrons

occupy molecular orbitals and a new configuration set in which one electron occupies a pseudo continuum orbital (PCO).

The PCOs are represented by an even-tempered basis set (Schmidt and Ruedenberg 1979 [55]) of GTOs centred at the centre of mass of the system, in which exponents of the GTOs are

EQ3.10:

$$\alpha_i = \alpha_0 \beta^{(i-1)}$$

which give different basis sets by changing the parameters α and β. These parameters much be chosen so that the electronic density of all target states involved in the close-coupling expansion are within the R-matrix box, so that the basis function amplitudes used to expand the molecular orbitals (MOs) vanish at the R-matrix boundary. Smaller values of β produce a more complete set of pseudostates but make it harder to avoid linear dependence. An extra orthogonalisation step is performed, Schmidt orthogonalisation of the PCOs to the MOs and then the PCOs are symmetric orthogonalised among themselves.

Chapter 4

R-Matrix Implementation

4.1 UKRmol

The implementation of the R-Matrix method used for this project is an evolution of the UK polyatomic R-Matrix code from Morgan et al 1998 [43] which in turn are based on additional older codes. They have being modified by many people over the years and have diverged into many different versions, with sub-modules that could no longer work due to incompatibility and no clear knowledge on how to use the modules beyond a very specific subset of parameters. During the course of this project an initiative was started to recombine and re-establish a core working set of UK R-matrix codes which is now known as the UKRmol suite and is available as freeware on http://ccpforge.cse.rl.ac.uk split into two projects UKRmol-in and UKRmol-out. CCPForge is a collaborative software development environment tool for the Collaborative Computational Projects. This chapter will give an overview of these projects using the diagrams this project contributed to the recent paper reintroducing the UKRmol suite [14] and descriptions of the individual modules also included in that paper.

UKRmol-in performs calculations for the inner region part of the calculation and is built on the 'Molecule-Sweden' quantum chemistry codes of Almlof and Taylor (1984) [3]. Figure 4.1 shows a flowchart describing the calculation of the target properties, the modules perform the following tasks:

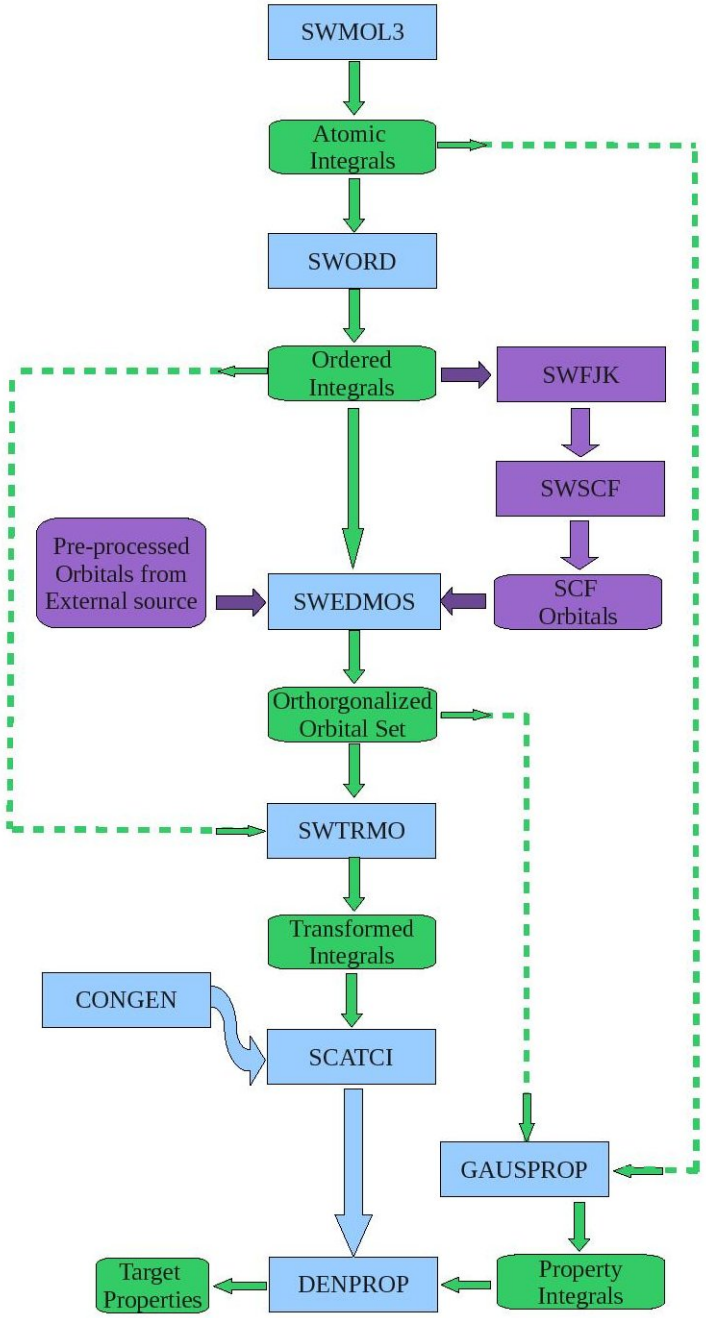

Figure 4.1: Flowchart for the target part of the calculation. The blue boxes indicate modules in the suite. The green boxes indicate the main output/input for the different modules. The purple boxes indicate alternative options to produce molecular orbitals in the calculation. Full arrows indicate the flow of the calculation, in particular those modules/input that feed into the following module in the suite. The dashed lines coming out of the green boxes indicate input for the modules.

SWMOL3 calculates the integrals between GTO basis functions that will be used later on. This program takes as input (in addition to a basis set) the geometry of the molecule and the point group it belongs to.

SWORD orders the calculated integrals.

SWFJK and SWSCF are run to obtain Hartree-Fock Self-Consistent-Field molecular orbitals. Nowadays, particularly for calculations involving several electronic states, it is usual to use orbitals obtained from more sophisticated methods (e.g. CASSCF) and external standard quantum chemistry codes. The program MPOUTRD has been developed to interface between MOLPRO [33] and the UKRmol suite.

SWEDMOS performs the orthogonalisation of the orbitals to be used in the calculation (which may not be the whole set generated, for example, in the HF-SCF step). The Schmidt technique is used for the orthogonalisation.

SWTRMO performs the transformation of the integrals labelled according to atomic orbitals to a set labelled over molecular orbitals.

CONGEN generates the configuration state functions (CSFs) to be used in the CI description of the target (even if a single-determinant description is chosen, this and the following program need to be run). The user input required in this program are the parameters defining the specific configurations to be built.

SCATCI builds the Hamiltonian matrix for the system using CSFs from CONGEN and the integrals transformed by SWTRMO. This Hamiltonian is then diagonalised to obtain the number of required eigenpairs.

GAUSPROP calculates property integrals for GTOs required by the next program.

DENPROP builds the density matrices for the target state(s) included in the calculation and determines the transition moments. This program can also calculate the polarisability of the target; although not used explicitly in the calculations, it can give an idea of the quality of the polarisation description in close-coupling calculations [36].

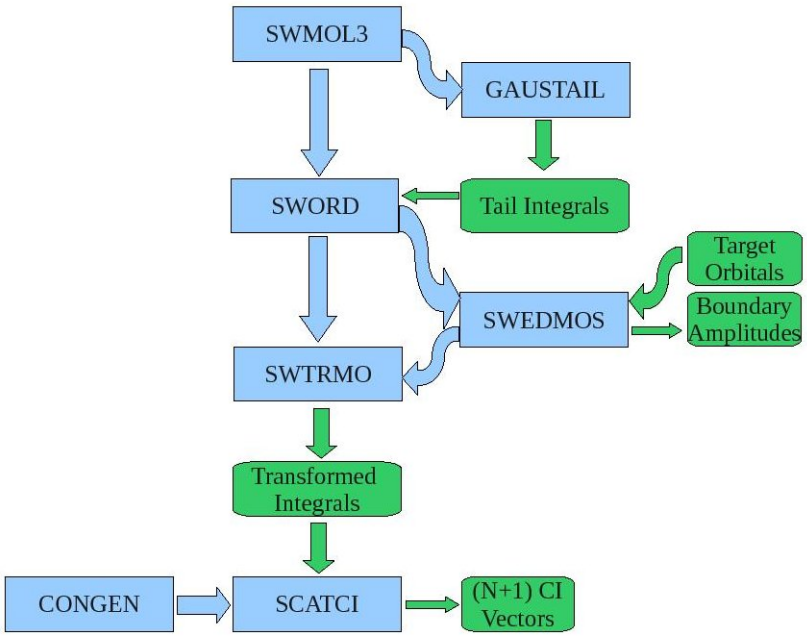

Figure 4.2: Flowchart for the inner part of the calculation. The blue boxes indicate modules in the suite. The green boxes indicate the main output/input for the different modules. Arrows indicate the flow of the calculation, in particular those modules/input that feed into the following module in the suite.

Figure 2 shows the flowchart of an inner region calculation. The same (but not all) programs as in the target calculations are used with the addition of GAUSTAIL. This program calculates the tail integrals, integrals between the boundary of the R-matrix sphere and infinity [20], that are then subtracted in SWORD from those generated in SWMOL3. GAUSTAIL requires as input the radius of the R-matrix sphere. The choice of radius also defines the continuum basis set that needs to be input to SWMOL3 in the inner region run.

When SWEDMOS is run in an inner region calculation, it performs two orthogonalisations: first, of the continuum basis set to the target molecular orbitals included in the calculation (and generated and/or orthogonalised in the target run). Then, the continuum orbitals are symmetric-orthogonalised among themselves. The program also generates the raw boundary amplitudes, that is the amplitudes of the continuum orbitals at the boundary between the regions (the amplitudes of the target orbitals are negligible by construction) necessary to build the amplitudes defined in equation (4).

In an inner region run, all eigenpairs are in principle required in SCATCI. Since the Hamiltonian for the system is block-diagonal (with P blocks, corresponding to all possible space-spin symmetries of the N +1 system), P runs of CONGEN and SCATCI are performed.

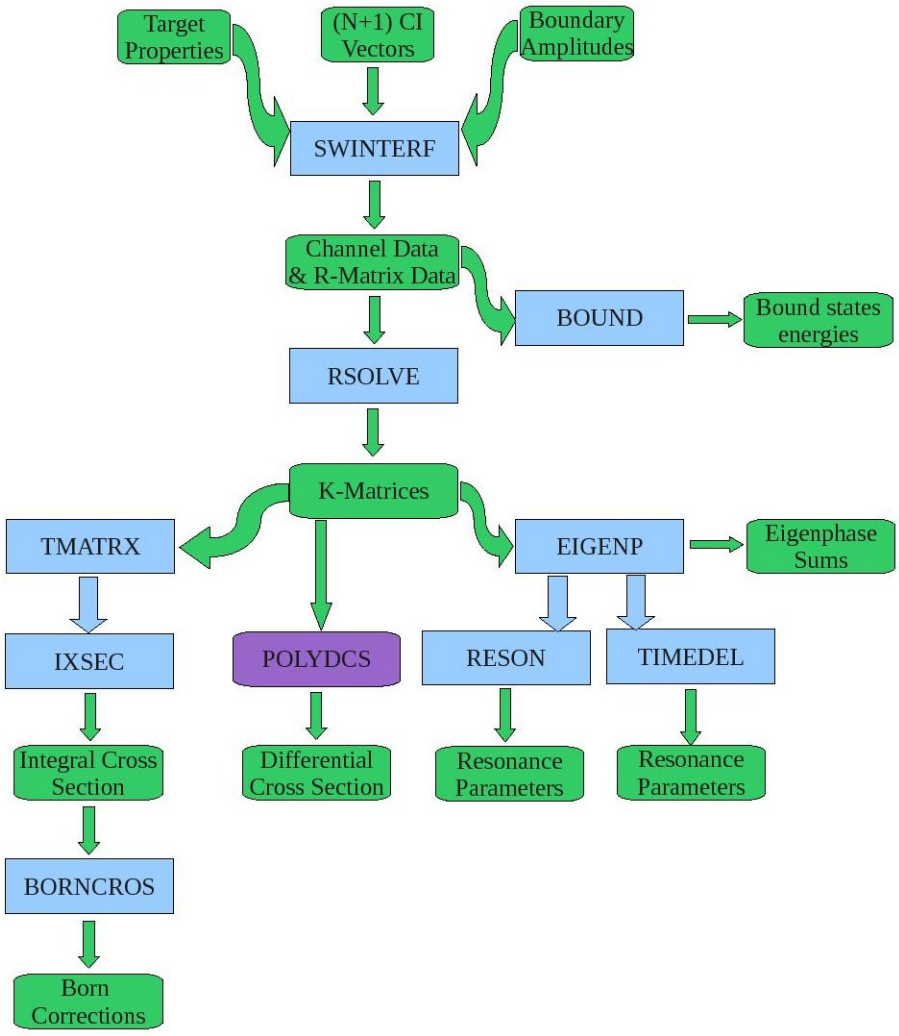

Figure 4.3: Flowchart for the outer part of the calculation. The blue boxes indicate modules in the suite. The green boxes indicate the main output/input for the different modules. Arrows indicate the flow of the calculation, in particular those modules/input that feed into the following module in the suite. PolyDCS is not part of the UKRmol suite, it was developed by Sanna and Gianturco[52]

Figure 3 shows the flowchart for the outer region calculation. As is the case for CONGEN and SCATCI, the outer region suite is run for each space-spin symmetry of the system. The programs involved are:

SWINTERF is an interface program that takes input from the target run (target properties) and inner region run (raw boundary amplitudes and eigenpairs) and produces two files containing channel data and data needed to build the R-matrix at the boundary between the regions. The user should indicate in the input how many of the target states included in the close-coupling expansion of the inner region are to be retained in the outer region calculation.

RSOLVE generates the K-matrices by building the R-matrix at the boundary between the regions and propagating it to a radial distance (normally a few tens of bohr) [35] where an asymptotic expansion provided by module CFASYM [36] can be used and the results then matched to asymptotic Coulomb or Bessel functions [37]. The scattering energies for which the scattering information is required must be specified here. Once the K-matrices are available several programs can be run to obtain different scattering quantities and observables.

EIGENP calculates the eigenphase sum by diagonalising the K-matrix.

RESON [38] uses the eigenphase sums to find and fit resonances to a Breit-Wigner profile in order to determine their energy and width. TIMEDEL [39] does the same, but using the time-delay method. Both programs work recursively in that they analyse the eigenphase sums for possible resonances and call RSOLVE at a suitable grid of energies before performing a fit.

TMATRX determines T-matrices from the K-matrices via simple matrix operations.

IXSEC calculates integral cross sections from T- matrices.

The K-matrices can be input into POLYDCS [40] to obtain electronically elastic differential cross sections, rotationally resolved integral cross sections and, also, to complete the partial wave expansion through the inclusion of a Born-type correction in the case of polar target molecules.

BORNCROS adds up the contribution of the different symmetries to obtain the integral cross section and also calculates an approximate Born correction both for electronically elastic and inelastic cross sections [41].

BOUND [42] finds bound states of the N + 1 system.

There are a number of programs, not included in the flowcharts, that are only run sporadically. For example, PSN is a program designed to obtain pseudonatural orbitals from the diagonalisation of density matrices obtained in DENPROP. The program can state average these orbitals using a set of user provided weights. Similarly CDENPROP [43] is a new code that calculates transition moments for the inner region wave functions. For the inner region calculation, it is necessary to have a GTO continuum basis set. In order to obtain one we use the following modules:

NUMCBAS evaluates Bessel and Coulomb functions within the R-matrix sphere.

GTOBAS [44] fits GTOs to he continuum functions generated by NUMCBAS. The exponents of GTOs are optimised using the method of Nestmann and Peyerimhoff [45].

In the outer region, the following programs are also available:
ALIGN [46] enables the treatment of collisions with oriented molecules.

MCQD [47] determines the multi-channel quantum defect for N + 1 states.

ROTIONS [48] calculates rotational excitation cross sections for linear ions.

ZEFF calculates the energy-dependent annihilation parameter Z_{eff} in the case of positron collisions using integrals computed in the inner region by GAUSDELTA [49].

4.2 Contributions to UKRmol

In order to carry out the CH^+ calculations it was necessary to have a complete and working set of codes for which the execution and input process was known. In order to achieve this we contributed to the UKRmol initiative. Some of the contributions were to support the CH^+ calculations and some were specific to helping the UKRmol initiative.

4.2.1 UKRmol-out Structure

Phase one of the UKRmol project was to cover the UKRmol-in modules with UKRmol-out to come at a later date. However as the CH^+ calculations would not be possible without a fully working outer region program, we brought together several of the diverged outer region codes into a single merged version. This involved a process of re-factoring functions and updating input and passed parameters of the functions in the code, followed by testing to make sure functionality remained correct. There is still some work remaining on updating MQDT and BOUND to be compatible with the modern core outer region modules but a core working set of modules now exist.

4.2.2 Integer Packing

Much of the original code dates back several decades and at that time memory management was a key requirement of scientific software development. As a carry over from that time, some parts of UKRmol-in used a technique called Integer Packing, where for example an 8-bit integer (which can hold numbers from 0-255), was used to store two 4-bit integers (which could hold values from 0-15). However with the progress of computers over time the integer packing methods were placing limits on how large a calculation the code could carry out. We searched the code modules for instances of integer packing and modified them to cope with greatly increased integer sizes and remove a bottleneck in running larger R-matrix calculations.

4.2.3 Diatomic Version

The original UK R-matrix codes were build to do calculations for diatomic molecules, the polyatomic code was build on the structures of that diatomic code and several modules are shared by both code streams. The diatomic code remained and while rarely used has the potential to be favoured over the polyatomic code when the focus is diatomic molecules. We updated the diatomic modules to be able to used the shared polyatomic modules that had received updates and modifications over the years.

4.2.4 Tools

One of the unfortunately common features of physics software and older physics software in particular, is that they often have unnecessarily complex input methods and the output streams do not present the relevant data in a desirable manner. This is true also for the UKRmol modules too, however several people have developed tools to help create the input for UKRmol-in based on the methods and information gathered by us. We also developed several tools to generate inputs for UKRmol-out and to extract relevant data from the output files generated by UKRmol-out. These tools are now provided as freeware along with the UKRmol suite on the 'ccpforge' software development environment.

4.2.4.1 IdTarg Generator

This tool allows the automatic generation of the idtarg input values that are required for the swinterf module in UKRmol-out, previous to this these values had to be calculated by hand which was a time consuming task and easily prone to errors.

4.2.4.2 Reson Extractor

The output file from UKRmol-out can often run to hundreds of megabytes of text, the vast majority of which are not relevant. The Reson Extractor tool searches this text automatically, extracting all relevant data on successfully identified resonances and stores this data in an immediately practical format that can input into imaging programs or data spreadsheets.

4.2.4.3 Polarisability

This tool take the output file from a target region run and calculates the polarisability of the molecule. Previously this data was only generated after the completion of the much longer inner region calculation.

4.2.5 QB Interface

The QB Interface module existed to be used as an interface for the QB resonance analysis code of Quigley and Berrington and was updated to work with the UKRmol generation of codes. The module was also modified to work as an interface between UKRmol and the PFARM project at Queens University Belfast. This involved re-factoring the code and updating functions to handle the same parameters now used by the UKRmol modules.

4.2.6 Positrons

One of the major undertakings of time spent on this project was to incorporate work into UKRmol, that expanded the older UK R-matrix codes to perform positron-molecule collisions and calculate the annihilation parameter Z_{eff}. These modifications were created by Rui Zhang [75] but unfortunately were done outside the UKRmol initiative. Over the course of four months we established a working set of codes used in the positron calculations, which had being built on parts of several diverse branches of the UK R-matrix

codes. Once a working set was established, we transitioned them through several branches and generations of the UK R-matrix codes until they were merged with the current UKRmol suite. Positron-molecule collisions and Z_{eff} calculations are now available through UKRmol on 'ccpforge' software development environment.

Chapter 5

Calculation Model

Calculating the rate of dissociative recombination of CH^+ under astrophysical conditions is difficult as the accurate prediction of excited state curve crossings is challenging. The key resonance curve appears to cross the ground state very close to the first vibrationally excited state. If previous experimental studies [2, 45, 24] had a small percentage of molecules in this vibrationally excited state, then their calculated recombination rates might significantly differ from what can be expected under conditions in interstellar clouds.

The aim of this project is to use the RMPS method to produce accurate resonance curves and crossing points for CH^+ . The first step was to decide on an RMPS calculation model, there were three requirements in selecting a model.

First it should produce polarisabilities that are close to accepted values, this is the strongest aspect of the RMPS method and what it greatly improves on over the standard R-matrix method.

Second it should produce energy curves that are close to accepted values, other calculation models have produced detailed CH^+ energy curves but do not go on to produce scattering calculations.

Finally the model needs to be computational viable with the resources available. The key variables to be choosen for our calculation model were the

size of the complete active space (CAS) configuration interaction (CI) space, the number of target states per symmetry and the values of the α and β exponents used to generate the pseudo continuum orbitals. The CH^+ target was represented using a cc-pVTZ basis set, a radius of 12 a_0 for the R-matrix box and keeping the two lowest electrons frozen for the calculations. The cc-pVTZ basis set was the largest that the current codes could accommodate, increasing the range of basis sets available to calculations models is one of the future aims of the UKRmol initiative.

5.1 Maximising Polarisability

A range of models were tested to see which would give the most accurate polarisabilities while being computationally viable. The tested CAS CI configurations ranged between the following:

$(1a_1)^2(2\text{-}3a_1,1b_1,1b_2)^3$ $(5\text{-}8a_1,2\text{-}3b_1,2\text{-}3b_2,1a_2)^1$

$(1a_1)^2(2\text{-}8a_1,1\text{-}3b_1,1\text{-}3b_2,\ 1a_2)^3$ $(9\text{-}20a_1,4\text{-}10b_1,4\text{-}10b_2,2\text{-}4a_2)^1$

All the calculations were carried out with the equilibrium internuclear separation of 1.127 Angstom.

MO	4110.0000	**States**	72
PCO	Varied	**Calculation**	RMPS
PCO	alpha xx	alpha zz	mean
11551	5.9394	7.8568	6.5785
14773	5.9777	7.8239	6.5931
16883	5.7986	7.7822	6.4598
1910104	5.8013	7.8006	6.4677

Figure 5.1: The polarisabilities for these CAS CI models showed little variability when the CAS CI was varied. Chosen model highlighted.

MO	4110	States	Varied
PCO	14773	Calculation	RMPS
States	alpha xx	alpha zz	mean
24	3.7061	0.1393	2.5172
32	3.7272	5.4086	4.2876
40	3.8123	5.4086	4.3444
48	4.2140	5.9763	4.8015
56	4.2577	7.5024	5.3393
64	4.2813	7.6171	5.3933
72	5.9777	7.8239	6.5931
80	6.0735	8.2952	6.8140
88	6.0753	8.2952	6.8153
96	6.0759	8.2952	6.8156

Figure 5.2: The polarisabilities for these CAS CI models showed large variability as the number of target states was increased. Chosen model highlighted.

MO	4110	States	80.0000
PCO	14773	Calculation	RMPS
(alpha, beta)	alpha xx	alpha zz	mean
(0.13, 1.4)	6.0735	8.2952	6.8140
(0.15, 1.4)	6.0735	8.2952	6.8140
(0.17, 1.4)	6.0735	8.2952	6.8140
(0.19, 1.4)	6.0735	8.2952	6.8140
(0.21, 1.4)	6.0735	8.2952	6.8140
(0.17, 1.0)	6.0735	8.2952	6.8140
(0.17, 1.2)	6.0735	8.2952	6.8140
(0.17, 1.4)	6.0735	8.2952	6.8140
(0.17, 1.6)	6.0735	8.2952	6.8140
(0.17, 1.8)	6.0735	8.2952	6.8140

Figure 5.3: Varying the alpha and beta values had negligible impact on polarisability values. Chosen model highlighted.

The model chosen for use in the main calculations was:
$(1a_1)^2(2\text{-}4a_1,1b_1,1b_2)^3$ $(5\text{-}14a_1,2\text{-}7b_1,2\text{-}7b_2,1\text{-}3a_2)^1$ with 10 states per symmetry, 80 states in total.
To determine how the RMPS method compared to standard R-matrix calculations in achieving accurate polarisabilities, we ran increasingly large R-matrix calculations until it could generate the same polarisability as the RMPS model, this eventually took a CAS of:
$(1a_1)^2(2\text{-}8a_1,1\text{-}3b_1,1\text{-}3b_2,1a_2)^4$
This R-matrix model generates 24,024 configurations compared to just 85 configurations needed by the RMPS model to produce similar polarisabilities.

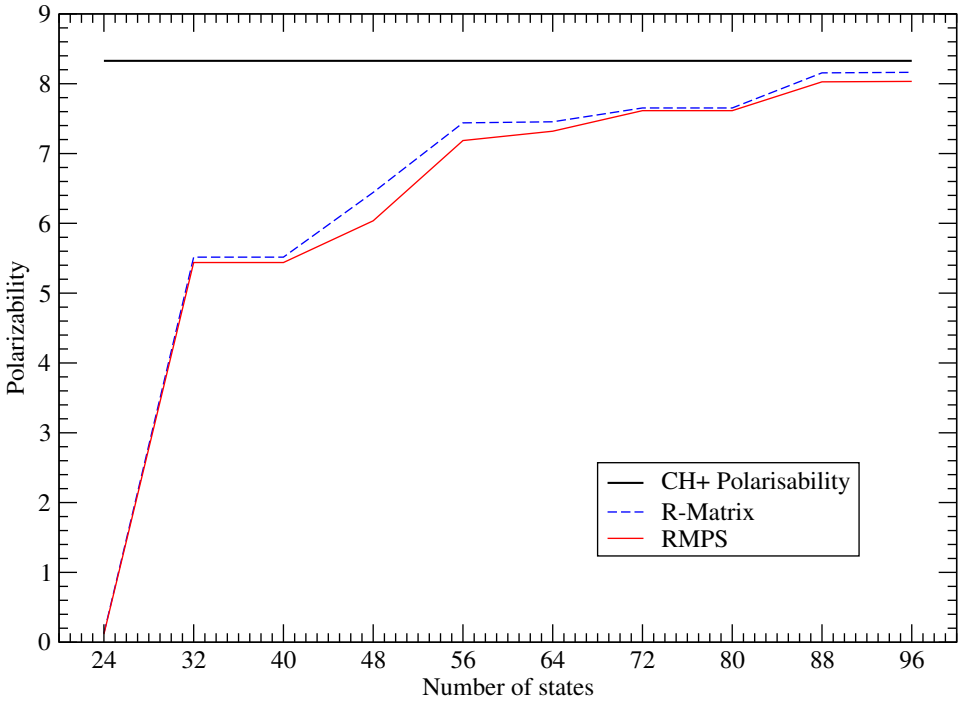

Figure 5.4: α_{zz} (also referred to as $\alpha_{\parallel}$) polarisability of CH^+ from the chosen RMPS model (requiring CAS CI 85 configurations) and the corresponding R-matrix calculation (which required 24,024 configurations). The black lines show the experimental α_{zz} values for CH^+ [16].

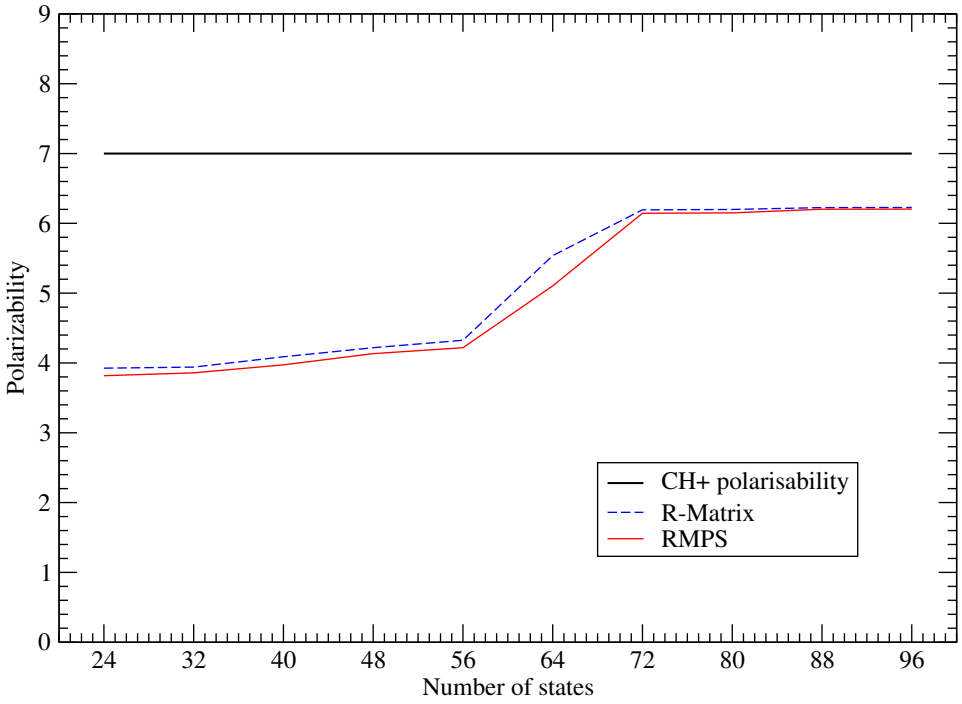

Figure 5.5: α_{xx} (also referred to as $\alpha_{\perp}$) polarisability of CH^+ from the chosen RMPS model (requiring CAS CI 85 configurations) and the corresponding R-matrix calculation (which required 24,024 configurations). The black line shows accepted α_{xx} values for CH^+ [16].

5.2 Energy Curve Convergence/Comparisons

To look at the CH^+ energy curves we compared our RMPS calculation model to an approximately computationally equivalent R-matrix model. We also compared the RMPS results to a recent detailed energy curve calculation by Barinvos and Van Hemert [4].

The CH^+ target was represented in the R-Matrix and RMPS calculations using a cc-pVTZ basis set, a radius of 12 a_0 for the R-matrix box and keeping the two lowest electrons frozen for the calculations. For the standard R-matrix calculation we used a complete active space (CAS) configuration interaction (CI) space of:
$(1a_1)^2(2\text{-}4a_1,1b_1,1b_2)^4$.
For the RMPS calculation we added a pseudo-continuum orbital basis of 10s,10p,6d orbitals, with exponents generated using α=0.17 and β=1.4. The RMPS configuration is:
$(1a_1)^2(2\text{-}4a_1,1b_1,1b_2)^3$ $(5\text{-}14a_1,2\text{-}7b_1,2\text{-}7b_2,1\text{-}3a_2)^1$.

The RMPS potential energy curves for CH^+ for the four lowest states: the X $^1\Sigma$ ground state, a $^3\Pi$, A $^1\Pi$ and b $^3\Sigma^+$ were compared with the standard R-matrix calculation. The RMPS run shows a clear improvement in these energy curves. In the R-Matrix data the $^3\Pi$ and $^1\Pi$ curves dissociate to a slightly lower energy than the $^3\Sigma$ and $^1\Sigma$ curves. In the RMPS run this divergence disappears and the four curves dissociate correctly to the same limit ($C^+(^2P)$ + $H(^2S)$).

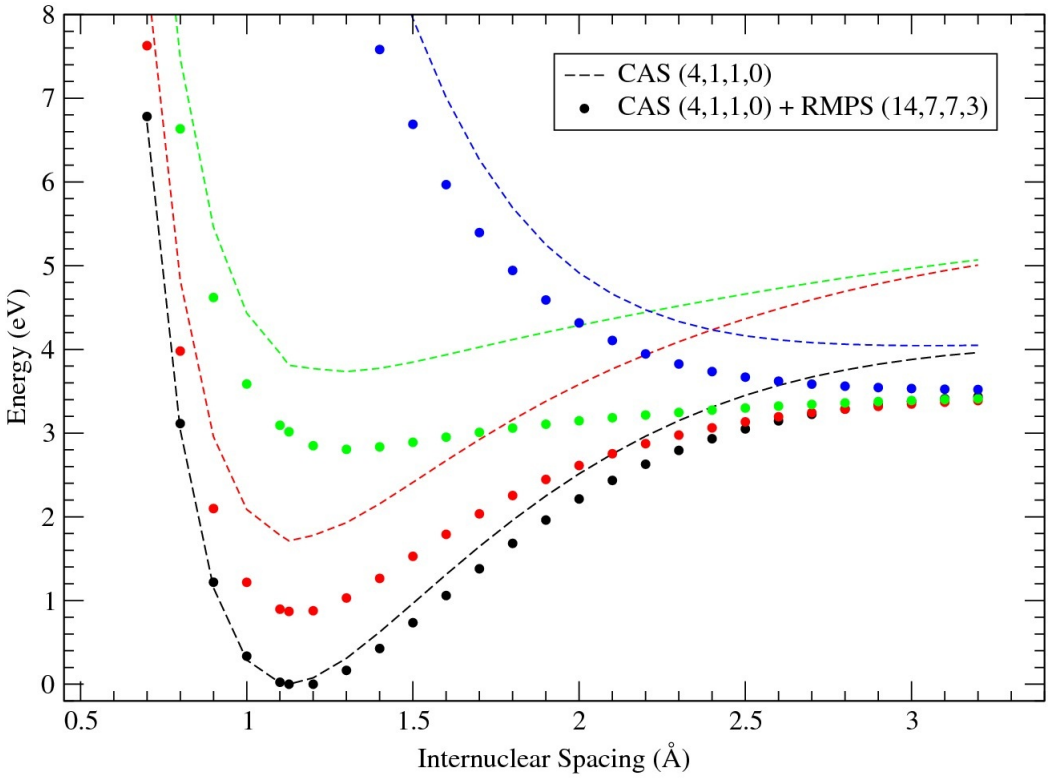

Figure 5.6: RMPS calculation and equivalent standard R-matrix calculation. Potential energy curves for the four lowest electronic states of CH^+ , showing the following states ascending in the order $^1\Sigma^+$, $^3\Pi$, $^1\Pi$ and $^3\Sigma^+$. In all cases zero energy has been set to minimum of the ground state.

The RMPS potential energy curves for CH^+ were then compared with electronic structure calculations of Barinvos and Van Hemert [4]. The calculations of Barinvos and Van Hemert [4] used a cc-pV6Z basis set with with added diffuse functions and polarisation functions to account for the core polarisation. The comparison of the RMPS calculation with these results confirms that the overall shape of our curves are broadly correct with a smaller calculation and smaller basis set (cc-pVTZ). The remaining discrepancy in the curves appears to be caused by the fact that our RMPS curves slightly underestimate the dissociation energy of CH^+ .

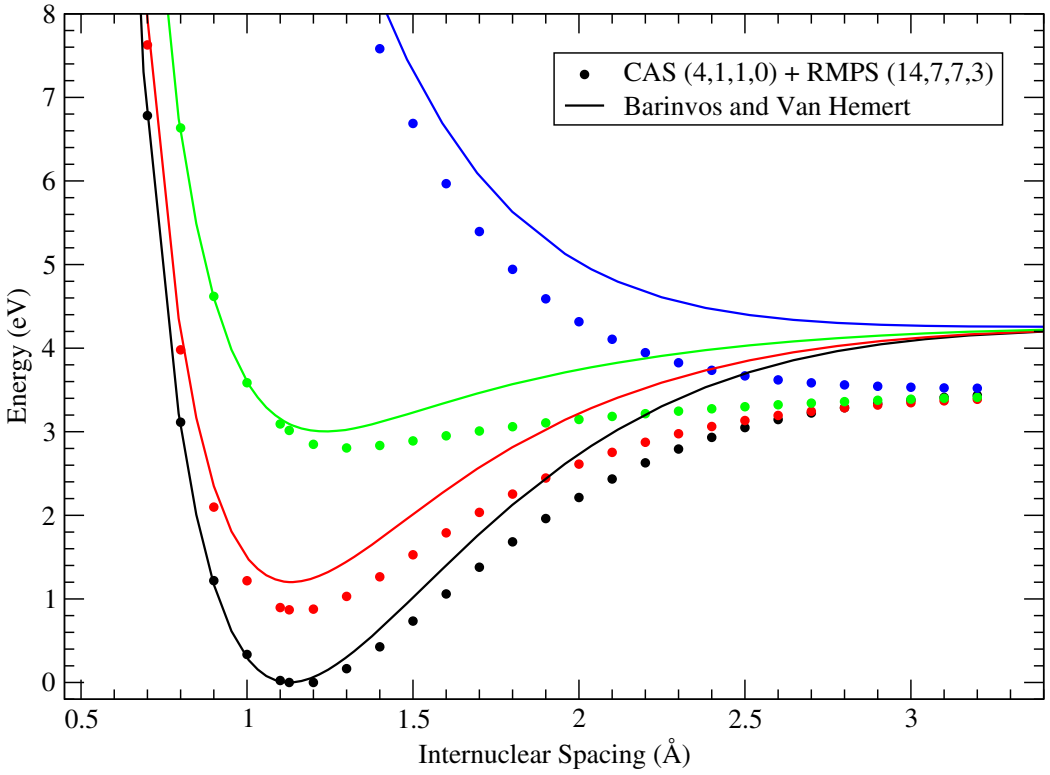

Figure 5.7: RMPS calculation and calculations by Barinvos and Van Hemert [4]. Potential energy curves for the four lowest electronic states of CH^+ , showing the following states ascending in the order $^1\Sigma^+$, $^3\Pi$, $^1\Pi$ and $^3\Sigma^+$. In all cases zero energy has been set to minimum of the ground state.

5.3 Calculation Requirements

The calculation was split into 43 internuclear separations between 0.7 and 3.2 Angstrom. For each internuclear separation an RMPS calculation was carried out for each of the doublet symmetries A_1, B_1, B_2, A_2. B_1 and B_2 are degenerate so calculations were only required for one. For each internuclear separation and symmetry combination, three resonance calculations were performed in ranges of 1.2 eV above the ground state energy, covering 0-3.6 eV. This gave a total of 387 calculations. Each required approximately 1.5 GB RAM and 4 GB of hard drive space and initially took approximate 140 hours on a single CPU core to complete, this put the total estimated computation time at 54,180 hours to be spread over 6-10 cores. However part way through the calculation series several new quad core computers (Intel i2500 CPUs) were installed in the research group network, each core of which could complete a calculation in 30 hours. The total computation time finished at approximately 23,000 hours and if run from the beginning on the newly available CPUs the projects calculations could be completed with approximately 11,600 hours of CPU time.

Chapter 6

Data and Results

In the main calculation the RMPS model retained 47 states, $6(^1\Sigma^+)$, $7(^3\Sigma^+)$, $8(^1\Pi)$, $9(^3\Pi)$, $5(^1\Sigma^-)$, $7(^3\Sigma^-)$, $3(^1\Delta)$, $2(^3\Delta)$, cutting off at 43.3 eV above the ground state. The outer region R-matrices were propagated to a radius of 100 a_0.

6.1 Resonances and Quantum Defects

Figure 6.1 shows eigenphase sums with $^2B_1$ ($^2\Pi$) symmetry for the RMPS calculations. The image shows the very complicated resonance structures as it converges on the first excitation threshold, a $^3\Pi$.

A challenge is presented by the need to resolve the dense collection of resonances just below the $^3\Pi$ threshold. The present calculations use the module in the UK R-Matrix polyatomic code called RESON [67] which automatically fits the eigenphase sums to a Breit-Wigner form in a recursive fashion. These resonance parameters are then used to generate complex quantum defects.

Analysis of the resonances using their effective quantum number with respect to the internuclear separation was carried out on a standard R-matrix calculation while the RMPS calculations were not yet complete. The graph in Figure 6.2 allowed us to identify 2 distinct series which we can tentatively

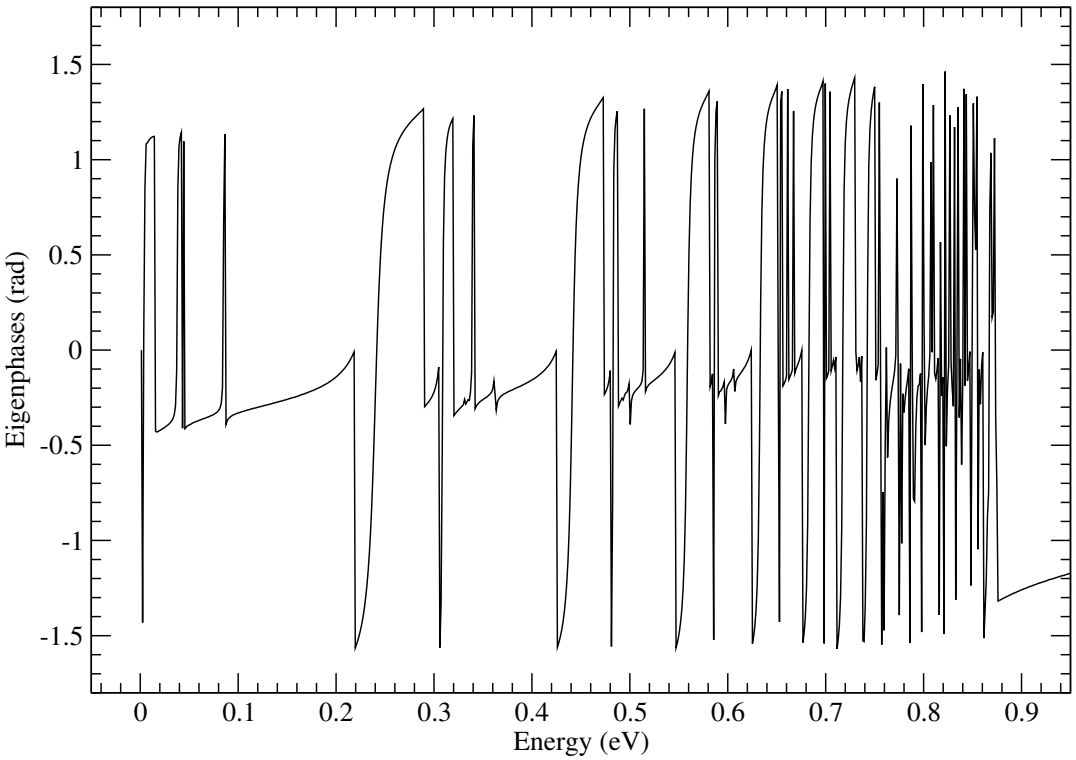

Figure 6.1: Eigenphases at equilibrium ($R = 1.127$Å) from the RMPS calculation.

assign as being the sσ and pσ series. Resonances associated with f and g waves have essentially zero quantum defect which means that their resonances coincide making them difficult to resolve with a Breit-Wigner fit. It was also not practical to clearly assign the dσ and dδ series. Overall this data display method did not produce enough reliable information and was not repeated for the RMPS data.

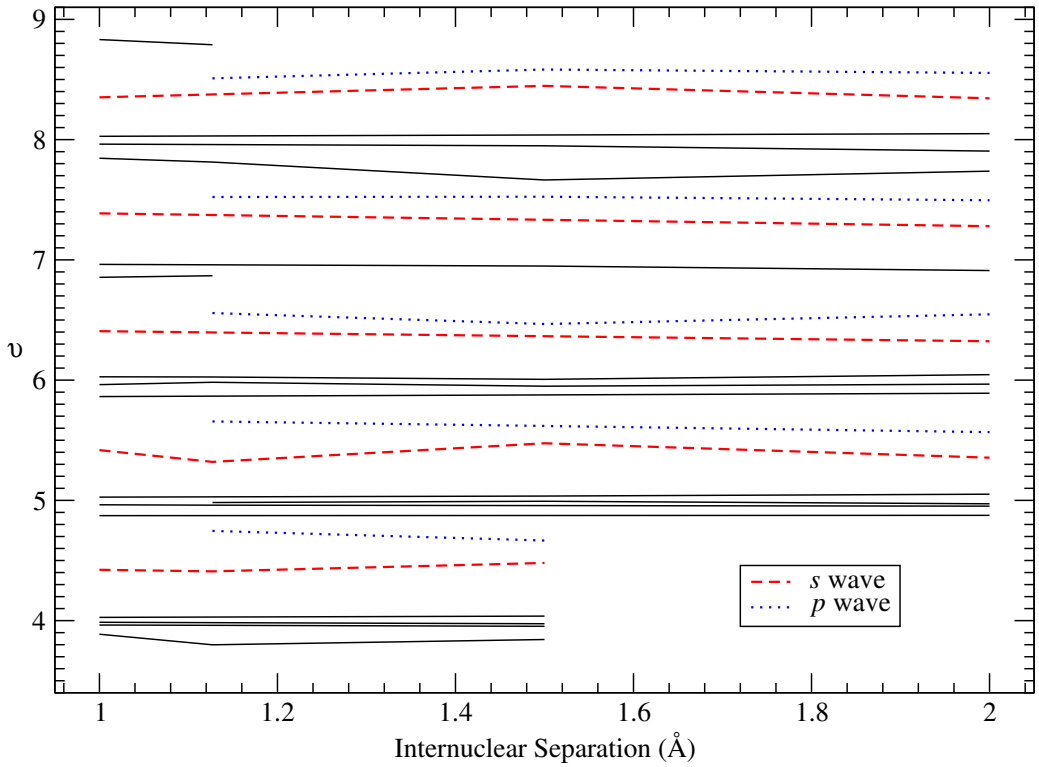

Figure 6.2: Effective quantum number, ν as a function of geometry for a standard R-Matrix calculation. The graph shows how our calculated quantum defects vary with bond length in R-Matrix calculations, the results shown in this figure are from a R-Matrix calculation that used the DZP basis set, a CAS of $(1a_1)^2$(4-8a_1,1-3b_1,1-3b_2,1-1a_2)^4 and retained 15 states in the scattering calculation.

6.1.1 Edlén plots

An alternative method of matching resonances below the $^3\Pi$ threshold between neighbouring geometries is to plot their quantum defects using Edlén plots. These plots show the quantum defects of each resonance against the resonance energies relative to the threshold energy. Figure 6.3 shows such plots for the sσ series for the RMPS calculation and also the standard R-

Matrix calculation that was used in Figure 6.2. These plots more clearly show the resonances for each symmetry at the equilibrium geometry (Figures 6.5 to 6.8). Neighbouring geometries can be matched up easily and for practical purposes we match using tables as opposed to drawing out each graph.

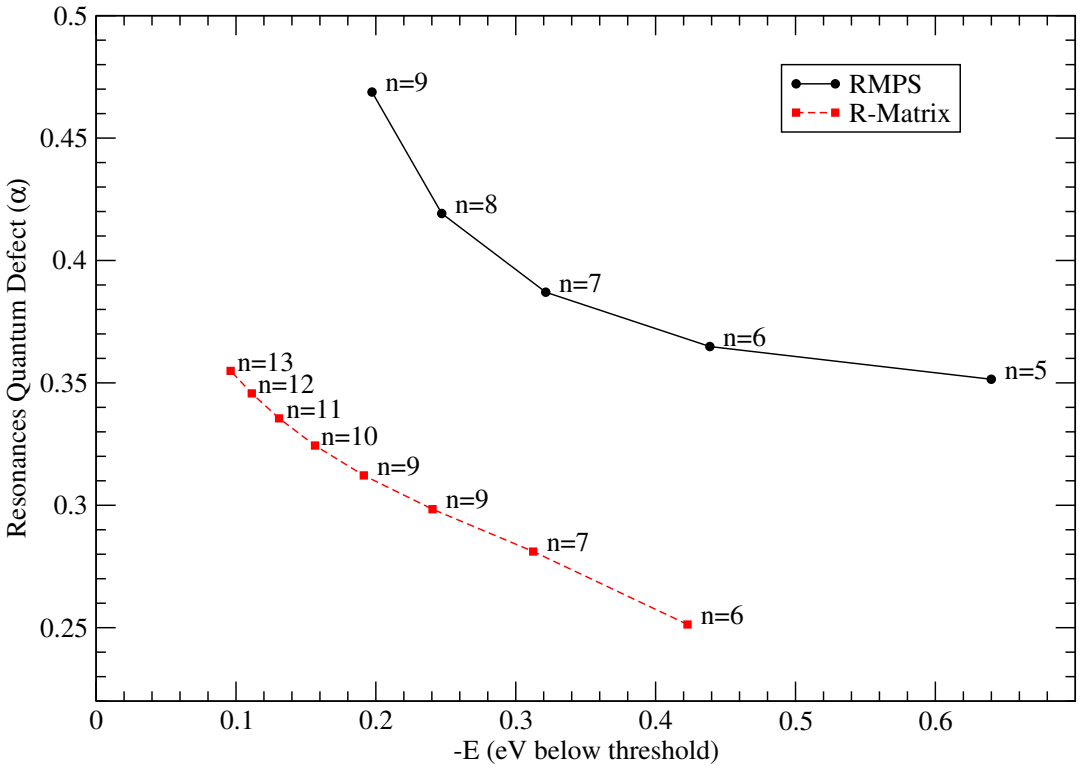

Figure 6.3: R-Matrix and RMPS Edlén plot at R=1.127 Å, for the $(a^3\Pi)ns\sigma$ series. The Edlén plot shows the quantum defects in order of descending effective quantum number, by plotting the quantum defect, α, against the resonance position below the threshold. The n values are the principle quantum numbers for the associated data point.

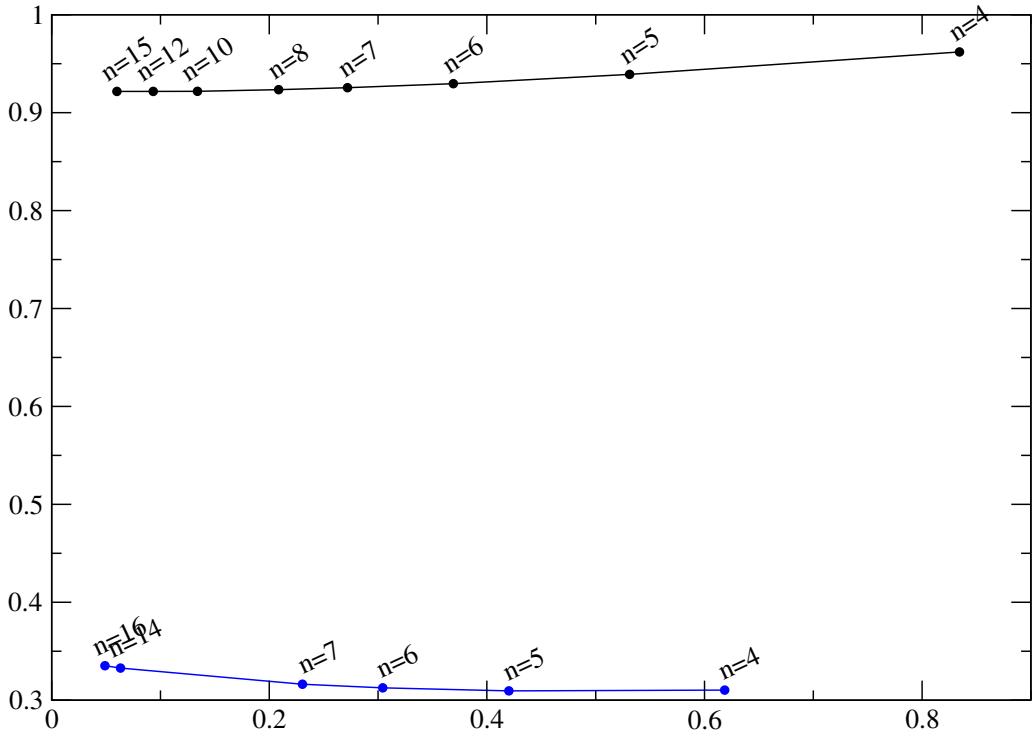

Figure 6.4: RMPS Edlén plot at R=1.127 Å, for doublet A_2 symmetry. The n values are the principle quantum numbers for the associated data point.

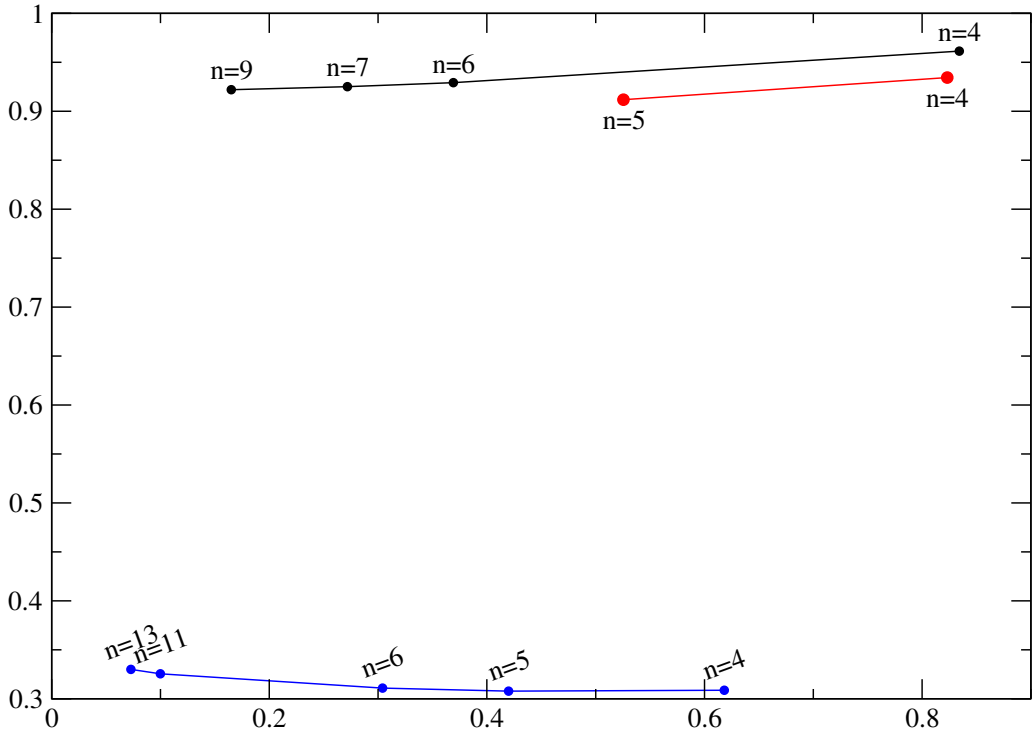

Figure 6.5: RMPS Edlén plot at R=1.127 Å, for doublet A_1 symmetry. The n values are the principle quantum numbers for the associated data point.

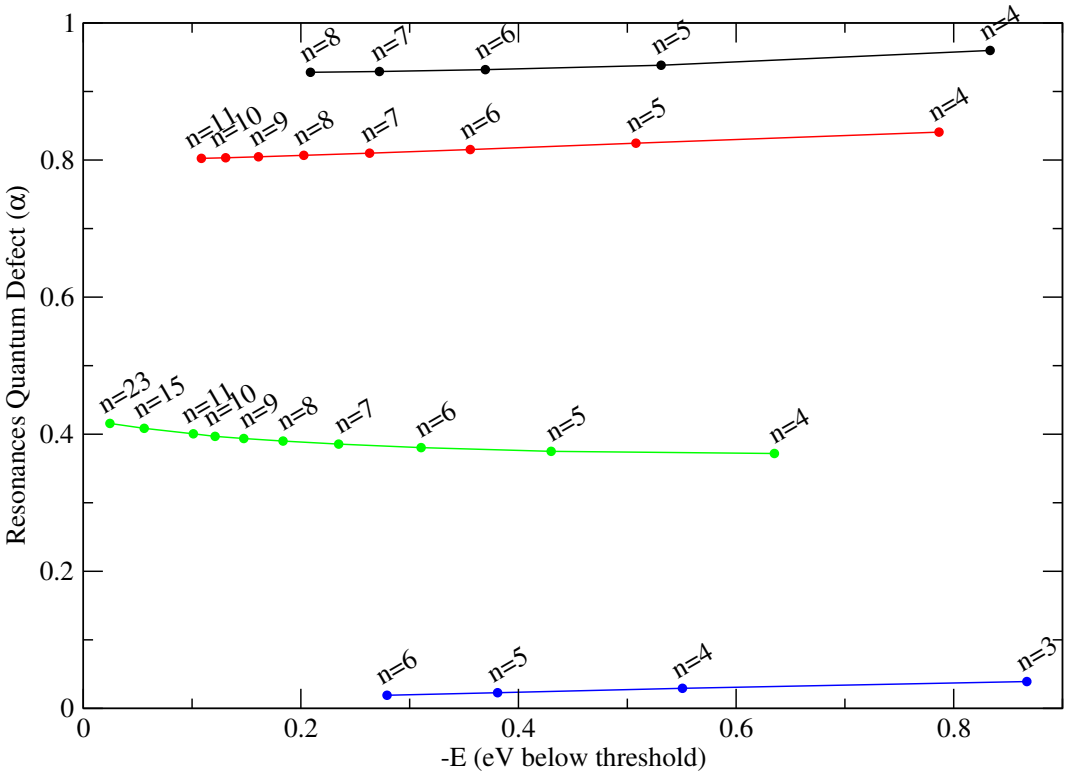

Figure 6.6: RMPS Edlén plot at R=1.127 Å, for doublet B_1 symmetry. The n values are the principle quantum numbers for the associated data point.

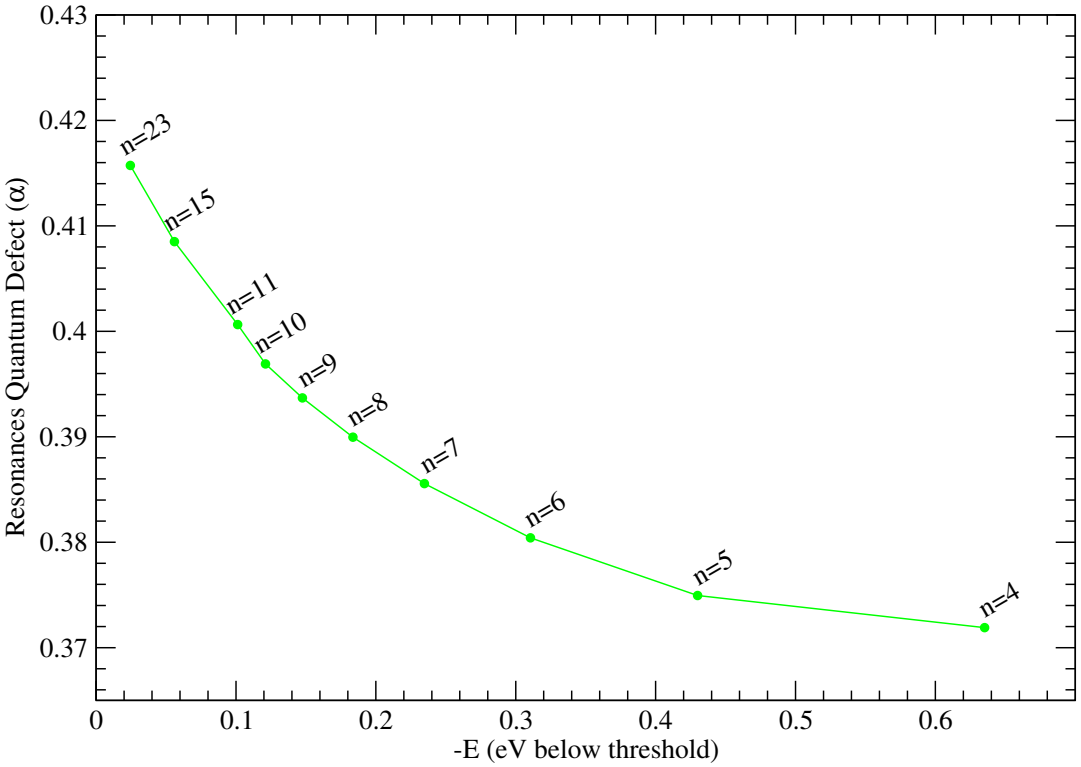

Figure 6.7: A closer look at one of the B_1 series from Figure 6.6. The n values are the principle quantum numbers for the associated data point.

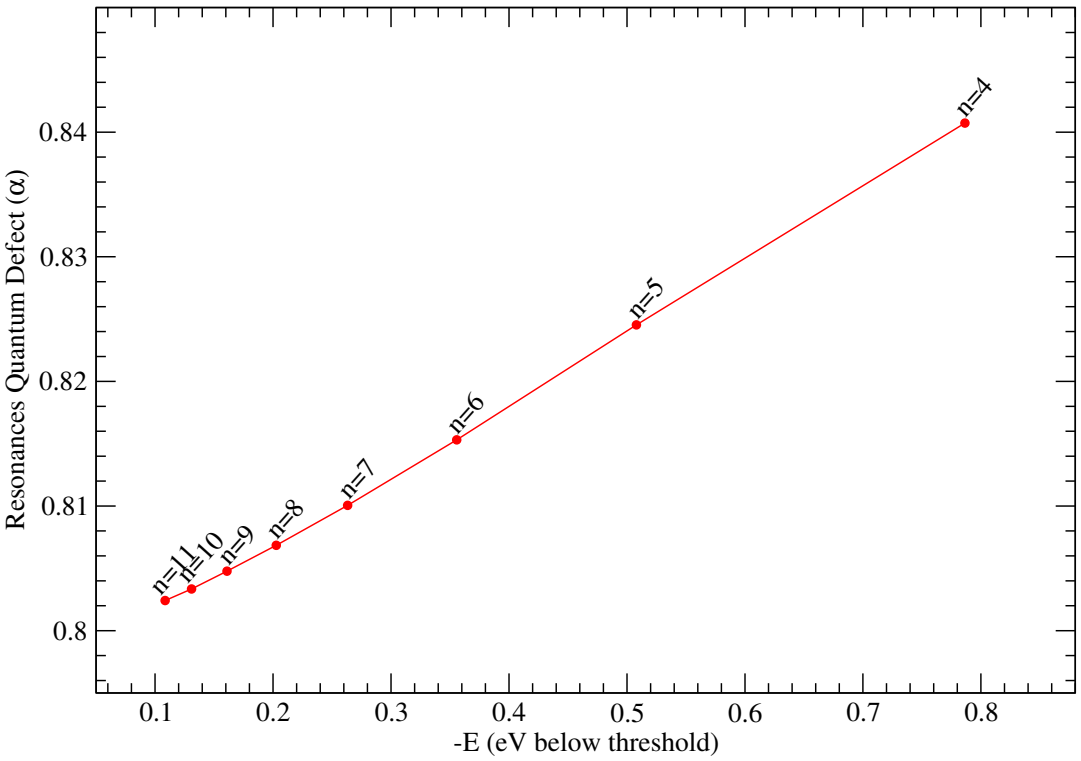

Figure 6.8: A closer look at one of the B_1 series from Figure 6.6. The n values are the principle quantum numbers for the associated data point.

GS-Equilbrium	-37.972583	-3.11	Edlen Plot (relative to threshold)	relative to GS-equilibirum	
Position	**Width**	**Quantum Defect (n-alpha)**	**-e**	**Position**	**Beta**
0.032242	0.000760	4.040266	0.8335	3.145746	0.000921
0.335135	0.000502	5.063891	0.5306	3.448640	0.001198
0.496767	0.000314	6.072697	0.3690	3.610272	0.001293
0.700677	0.000107	9.080087	0.1651	3.814181	0.001474
0.786184	0.000034	13.081232	0.0796	3.899688	0.001389
0.246981	0.000560	4.689280	0.6188	3.360486	0.001061
0.445658	0.000385	5.691257	0.4201	3.559163	0.001304
0.685329	0.000136	8.685174	0.1804	3.798834	0.001642
0.746459	0.000078	10.682065	0.1193	3.859964	0.001741
0.765980	0.000060	11.680994	0.0998	3.879484	0.001768
0.822137	0.000025	17.674301	0.0436	3.935642	0.002551

GS-Equilbrium	-37.972583	-0.34	Edlen Plot (relative to threshold)	relative to GS-equilibirum	
Position	**Width**	**Quantum Defect (n-alpha)**	**-e**	**Position**	**Beta**
0.046500	0.001082	4.038010	0.8344	0.382420	0.001309
0.349699	0.000655	5.060904	0.5312	0.685619	0.001561
0.511676	0.000455	6.070383	0.3692	0.847596	0.001870
0.609041	0.000308	7.074462	0.2719	0.944961	0.002006
0.672310	0.000215	8.076503	0.2086	1.008229	0.002083
0.746933	0.000116	10.078201	0.1340	1.082853	0.002182
0.787621	0.000070	12.078283	0.0933	1.123541	0.002254
0.821040	0.000037	15.078332	0.0599	1.156959	0.002325
0.262281	0.000681	4.689698	0.6186	0.598201	0.001291
0.460736	0.000460	5.690497	0.4202	0.796656	0.001557
0.576664	0.000314	6.687412	0.3043	0.912583	0.001723
0.650442	0.000220	7.683735	0.2305	0.986362	0.001838
0.817638	0.000040	14.667222	0.0633	1.153558	0.002294
0.831891	0.000026	16.664848	0.0490	1.167811	0.002248

Figure 6.9: Two tables each showing two resonances identified by quantum defect for RMPS calculations at R=0.8 (upper) and R=1.0 (lower) Angstroms respectively

6.2 Resonance Crossings

We have completed calculations of our energy curves and resonance data using the RMPS method on the CH^+ system. Using this data we now draw the resonance curves to allow more accurate resolving of the crossing points of key resonances with the energy curves.

Figures 6.10 shows the four lowest states of CH^+ and the red curves show the three lowest resonance curves. Figures 6.11 and 6.12 show a zoomed in view of these resonance curves and their crossing points. Figure 6.13 adds the vibrational levels and we can see in Figure 6.14 how the first resonance crosses just above the first vibrational level.

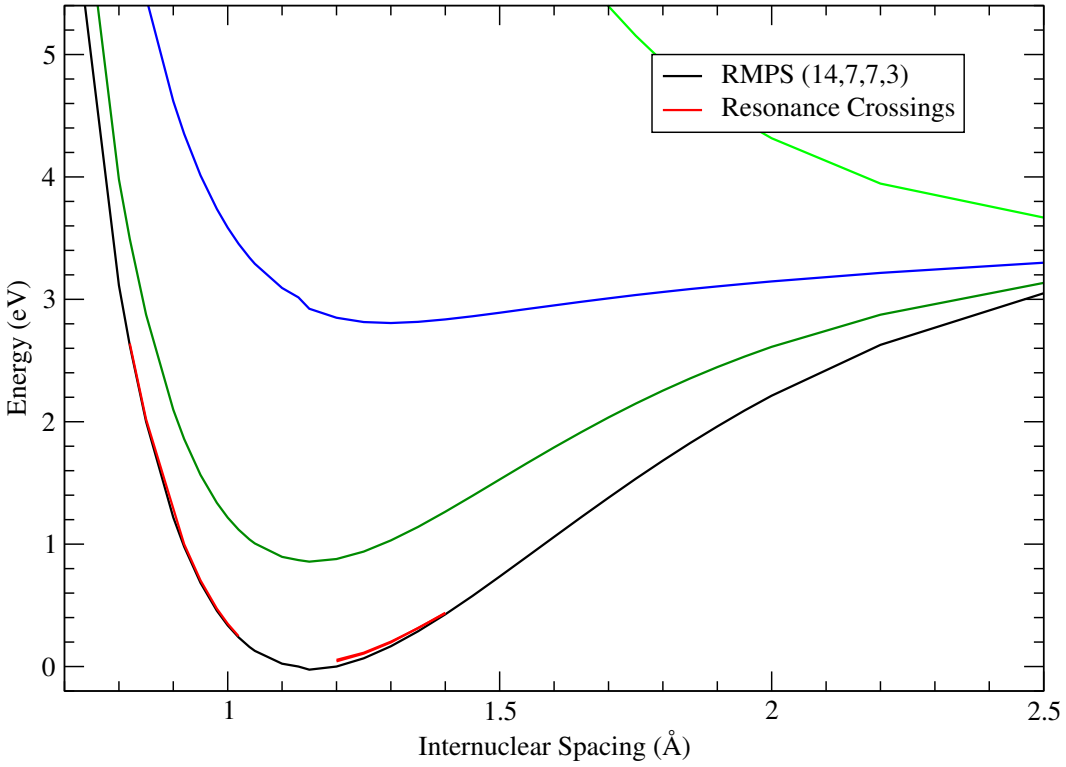

Figure 6.10: RMPS Energy curves and two resonance curves in red.

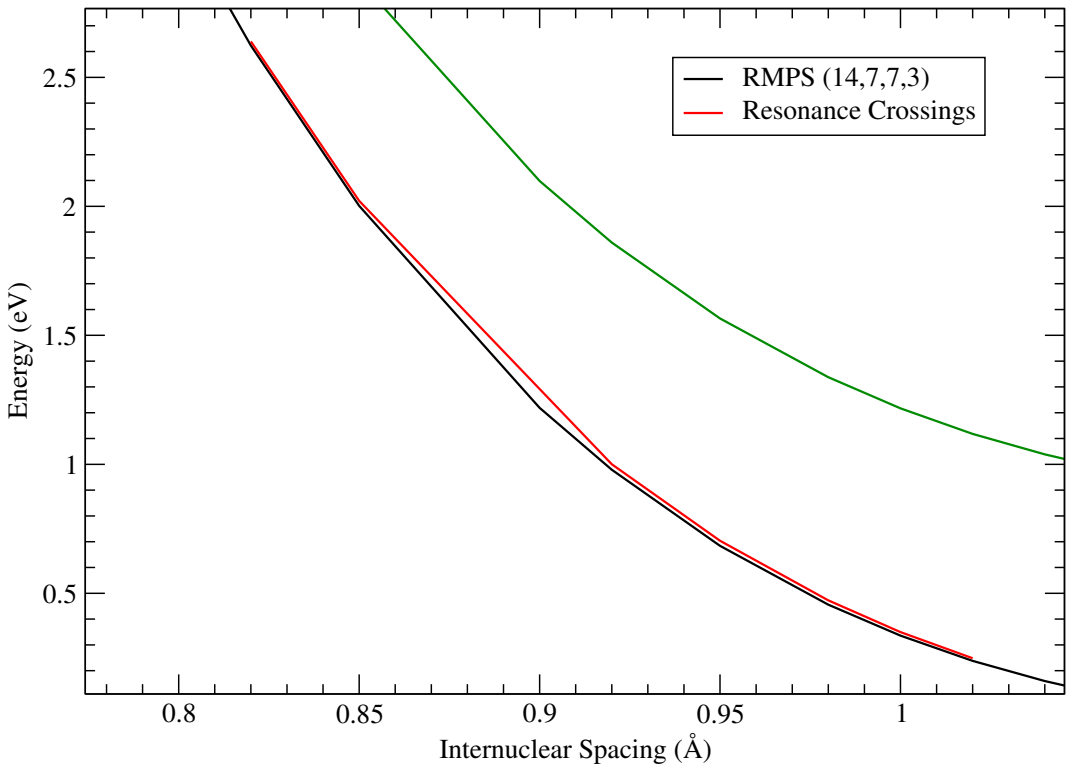

Figure 6.11: A zoomed in view of the first resonance curve (red solid line), the ground state curve (black solid line) and the first excited state (green solid line).

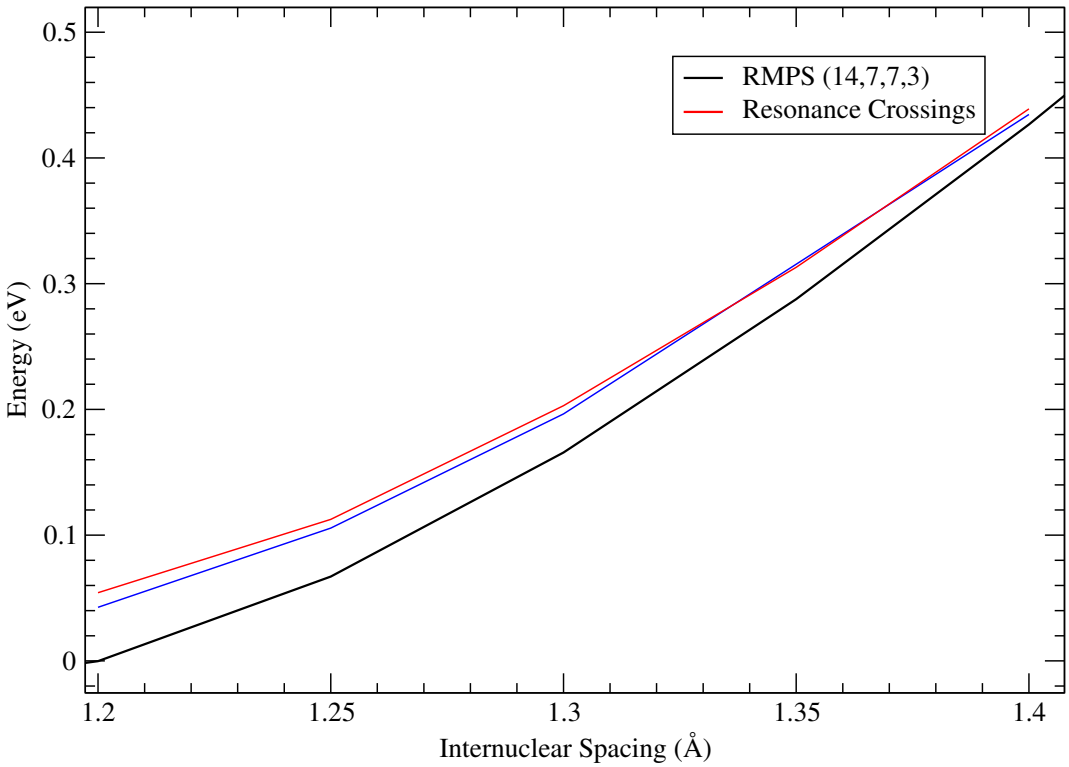

Figure 6.12: A zoomed in view of the second (blue solid line) and third (red solid line resonance curve) with the ground state curve (black solid line).

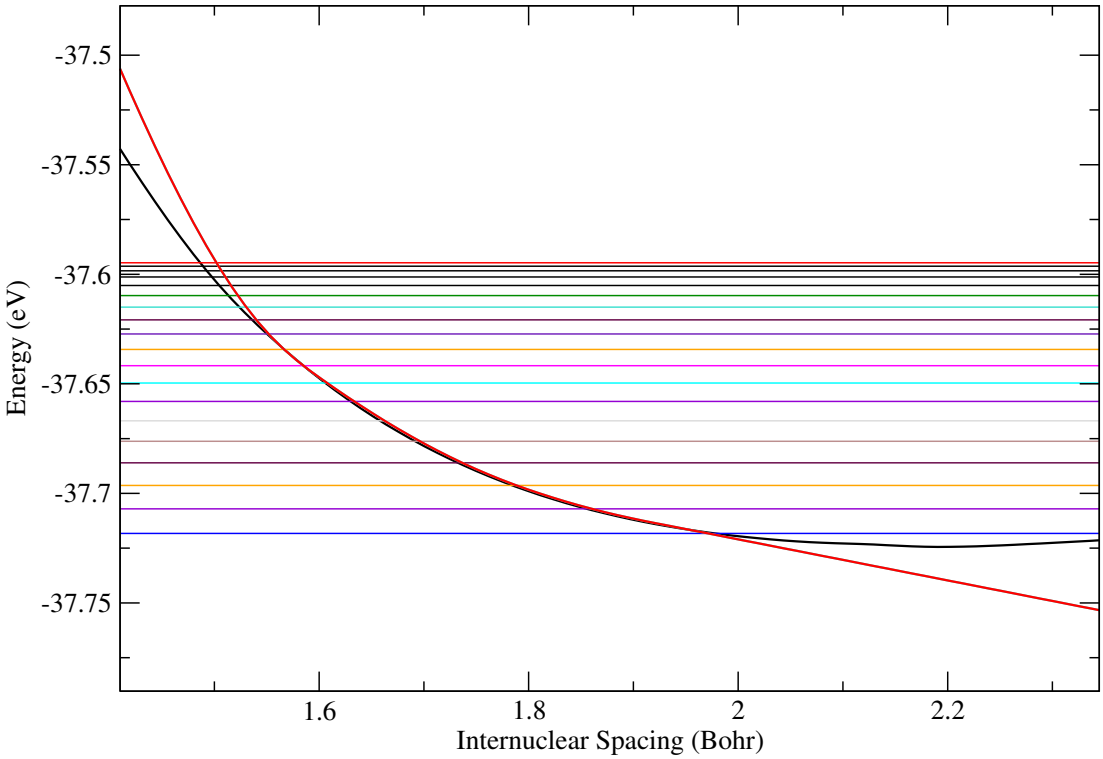

Figure 6.13: The ground state curve (black solid line) along with the first resonance curve (red solid line). Along with the vibrational levels (horizontal lines).

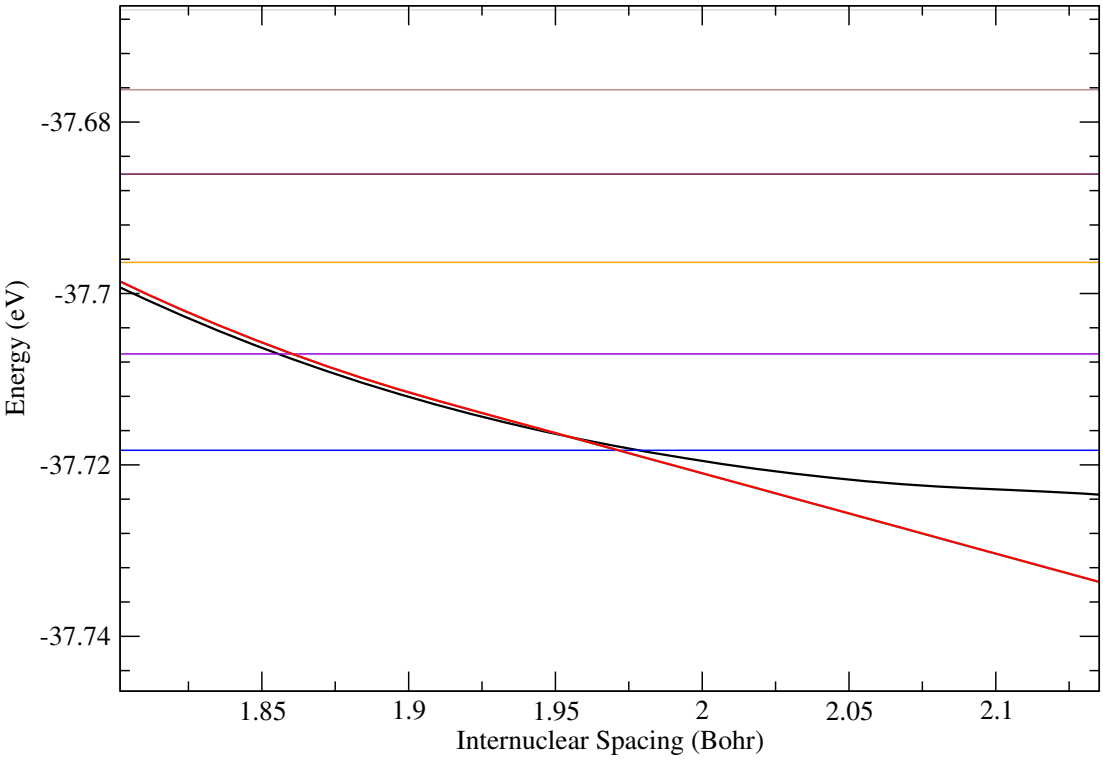

Figure 6.14: A zoomed in view of Figure 6.12 where we can see the first resonance (in red) crossing the ground state curve (in black) just higher than the first vibrational level (in blue).

6.3 Resonance Curve Comparisons

With our calculated energy curves and resonances we need to compare our results to existing data. Figure 6.13 shows a lot of data at once, but once the parts are identified, it shows clearly the value of these calculations.

The figure shows the CH^+ ground state energy curve for our RMPS calculation as a solid black line, with the two resonance crossings in dashed red. This corresponds to a subset of Figure 6.10. Almost on top of the RMPS ground state is another curve of black dots, this is the ground state curve from Hemert's data [4], that was previously shown in Figure 5.4. We can clearly see in 6.15, that those two ground state covers are very similar in the area of the first resonance curve. Finally 6.15 shows in blue the ground state curve from Carata [13] and in gold the two lowest resonance curves they calculated for CH^+ .

The Carata ground state curve is not a close match for the Hemert curve, which was a calculation focused on generating an accurate set of CH^+ energy curves. This suggests that as the RMPS ground state curve is a closer match to the Hemert one (though it still has room for improvement), and hence that our resonance curves will also produce more accurate resonance crossing positions and hence a more accurate dissociative recombination calculation.

The second aspect of the image to consider are the two resonance curves for both the RMPS calculation and the Carata calculation. The first (leftmost) resonance curve for both calculations has similar positions relative to their respective ground state curves and similar positioning has being seen in other CH^+ calculations [2][31][13][65]. The second resonance curve from the Carata calculation has an unexpected position. While we only show the two lowest resonance curves from our RMPS data, we recorded many additional resonances between the ground state and 1st excited state, each of which follow roughly the shape of the ground state curve. The Carata second resonance does not follow the shape of its respective ground state curve and this would impact on the position of subsequent resonances. However to

determine for certain which set of data is more accurate we need to look at the dissociative recombination cross sections.

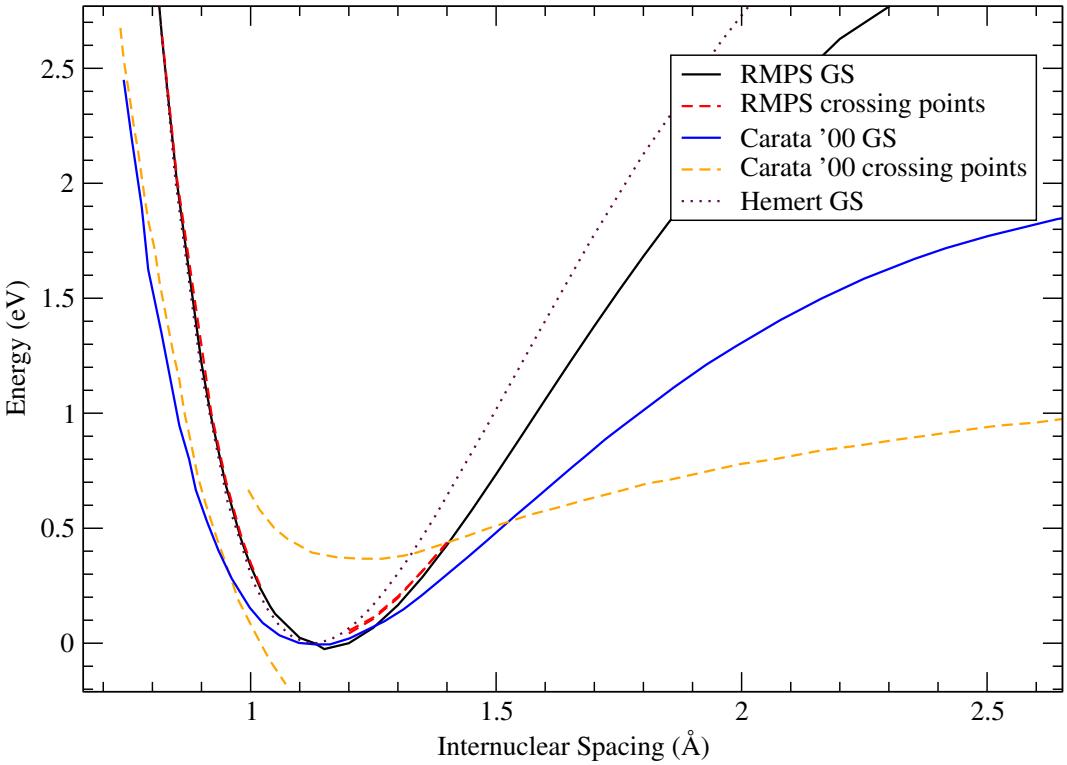

Figure 6.15: Comparison of energy curves from our RMPS calculation (black solid line) with energy curve from Carata [13](blue solid line) and Hemert [4](black dotted line). Also shown are two low lying resonance crossing curves generated by RMPS (red dashed lines) and the same curves by Carata (orange dashed lines).

6.4 Couplings and Dissociative Recombination Cross Sections

We applied multi-channel quantum defect theory (MQDT) to generate the dissociative recombination (DR) cross sections using software developed by Ioan Schneider in Le Harve, France. The inputs for this program were the CH^+ energy curves, the resonance couplings, a function of the resonance widths, and the resonance positions.

The widths for the resonance is converted to couplings using: $\sigma = \sqrt{\frac{\Gamma}{2\pi}}$ Figure 6.16 shows the coupling data generated for the first resonance and Figure 6.17 shows how this data (red points) is incorporated into a continuous data stream for the MQDT program. To generate the continuous data stream we allow either side of the couplings to fall off to zero over a distance of 1 bohr using a Gaussian form.

Calculations were repeated with variations of this extrapolation. Increasing the distance the Gaussian drop off occurred from 1 bohr to 2.5 bohr showed no variation in the final cross section. Reducing the fall off distance, to below 1 bohr, does cause the final cross section to decrease and with a 0.2 bohr fall off the cross section decreases by a full order of magnitude. We remained with a fall off of 1 bohr as this is the recommended practice for the software provided [56]. But it is worth investigating in future the justification of choosing that fall off.

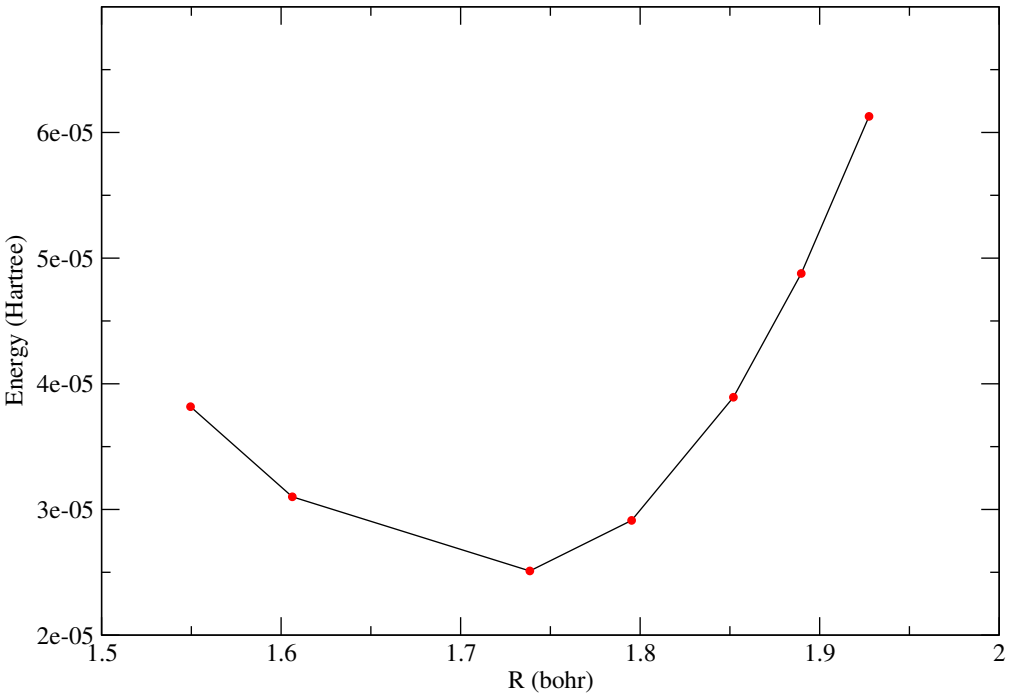

Figure 6.16: Couplings for the first resonance curve.

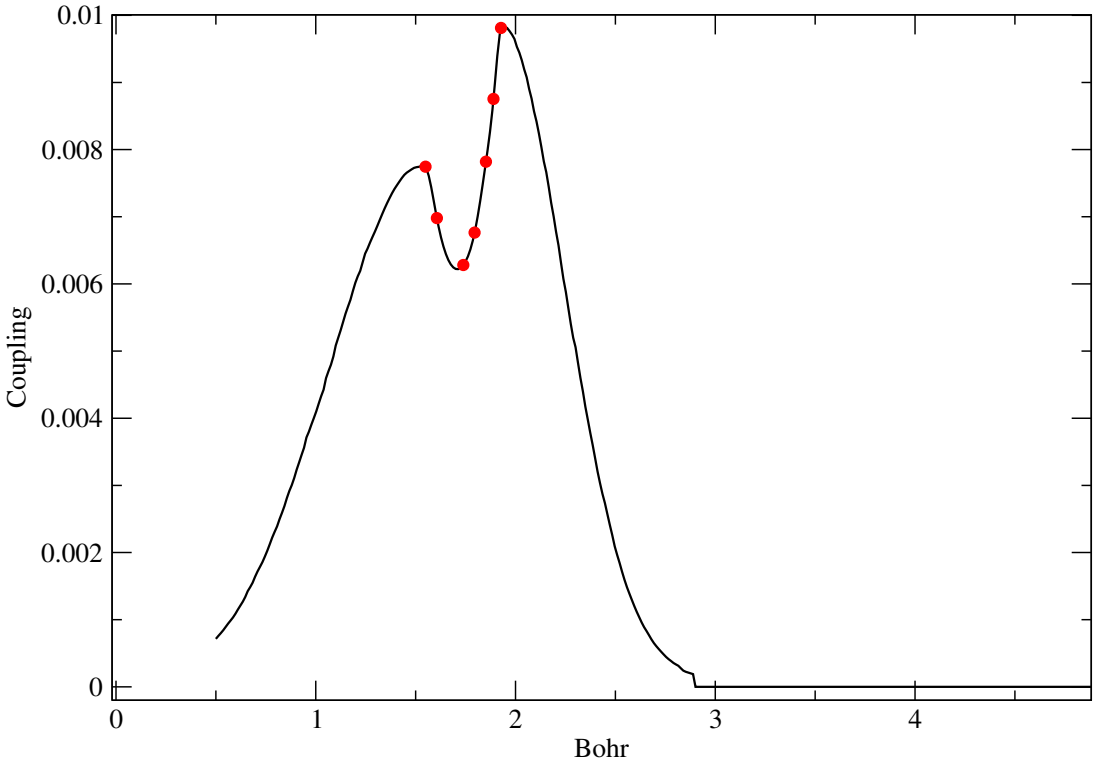

Figure 6.17: The resonance curve widths in Figure 6.17 are converted to couplings (red dots). The black curve is the extrapolated coupling curve data used in the dissociative recombination calculation. This extrapolation is done following the method of Schneider [56]

Figure 6.18 shows the final calculated dissociative recombination cross section for CH^+ . This is within a factor of two of the experimental data from the heavy-ion storage ring data of Amitay and Zaifman [2].

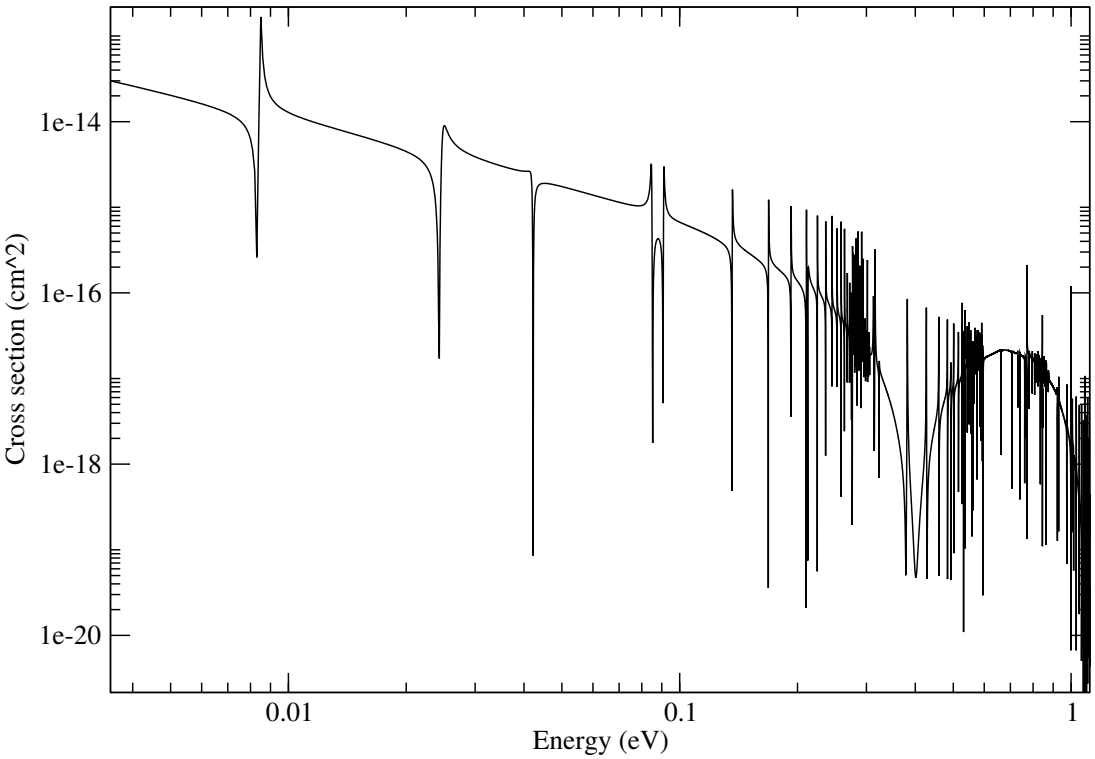

Figure 6.18: The CH^+ Dissociative recombination cross section based on the RMPS data.

Chapter 7

Summary

7.1 Analysis of CH^+ RMPS calculations

We have completed the RMPS calculations for CH^+ and generated data for energy curves, resonance curves resonance widths for internuclear separations of 0.7 to 3.2 Angstrom and up to 3.6 eV above the equilibrium ground state. This data compares well to existing detailed energy curves by Hemert [4] and improves on recent similar calculations by Carata [13].

We have carried out an initial dissociative recombination calculation, in association with Ioan Schneider in Le Havre, France, using the dissociative recombination codes that exists there. A more detailed dissociative recombination analysis is to be continued by Ioan Schneider, using the RMPS data calculated by this project.

A paper on the early results from this project has being published in the J. Phys: Conf. Series [39]

7.2 Contributions to UKRmol

We have contributed in the creation of the UKRmol suite of R-Matrix programs. Organising a core set of working out region codes in UKRmol-out, improving the integer packing methods in UKRmol-in, creating a series of tools to enhance the use of UKRmol-out and contributing knowledge and design in the creation of a similar series of tools for UKRmol-in. QB Interface has being updated to play a vital link between UKRmol calculations and the calculations from the PFARM project in Belfast. The older diatomic code has being updated to a working version for those who want to use it. Perhaps most valuable in the long term is the incorporation of the positron and Z_eff work by Rui Zhang into the modern UKRmol codes, ensuring its continued use in future.

Bibliography

[1] http://ccpforge.cse.rl.ac.uk/gf/project/ukrmol-in/

[2] Amitay Z, Zajfman D, Forck P, Hechtfischer U, Seidel B, Grieser M, Habs D, Repnow R, Schwalm D and Wolf A 1996 *Phys. Rev. A* **54** 4032

[3] Almlof J and Taylor P R 1984 *Advances theories and computational approaches to the electronic structure of molecules*

[4] Barinovs G and van Hemert M C 2004 *Chem. Phys. Lett.* **399** 406–411

[5] Bradsley J N and Junker B R 1973 *Astrophys. J.* **183** L135-137

[6] Bartschat K and Hudson and Scott MP and Burke PG and Burke VM 1996 *J. Phys. B: At. Mol. Opt. Phys.* **29** 115-123

[7] Bates D R and Spitzer L 1951 *Astrophys. J.* **113** 441-463

[8] Bloch C 1957 *Nucl. Phys.* **4** 503-528

[9] Burke P G and Robb W D 1975 *Adv. At. Mol. Phys.* **11** 143214

[10] Burke P G 1976 *Proc. 5th Int. Conf. on Atomic Physics* p.293

[11] Burke P G, Mackey I and Shimamura I 1977 *J. Phys. B: At. Mol. Opt. Phys.* **10** 24972512

[12] Burke P G, Hibbert A and Robb W D 1971 *J. Phys. B: At. Mol. Opt. Phys.* **4** 153161

[13] Carata L, Orel A E, Raoult M, Schneider I F and Suzor-Weiner A 2000 *Phys. Rev. A* **62** 052711

[14] Carr J M and Galiatsatos P G and Gorfinkiel J D and Harvey A G and Lysaght M A and Madden D and Masin Z and Plummer M and Tennyson J and Varambhia H N 2012 *Eur. Phys. J. D* **66** 58

[15] Charlton M, Griffith T C, Heyland G R and Wright G L 1983 *J. Phys. B: At. Mol. Phys* **16** 323–341.

[16] Christiansen O and Hattig C and Gauss J 1998 *J. Chem. Phys* **109** 4745-4757

[17] Danby G and Tennyson J 1990 *J. Phys. B: At. Mol. Opt. Phys.* **23** 1005–1016 erratum 23, 2471 (1990)

[18] des Forets P and Flower G and Hartquist DR and Dalgarno A 1986 *Mon. Not. R. Astr. Soc* **220** 801–824

[19] Douglas A E and Herzberg G 1941 *Astrophys. J.* **94** 381

[20] Faure A and Tennyson J 2002 *J. Phys. B: At. Mol. Opt. Phys.* **35** 1865–1873

[21] Faure A, Gorfinkiel J D, Morgan L A and Tennyson J 2002 *Computer Phys. Comms.* **144** 224241

[22] Feshbach H 1658 *Ann. Phys. (N.Y.)* **5** 357

[23] Feshbach H 1658 *Ann. Phys. (N.Y.)* **19** 287

[24] Forck P, Broude C, Grieser M, Habs D, Kenntner J, Liebmann J, Repnow R, Amitay Z and Zajfman D 1994 *Phys. Rev. Lett.* **72** 2002–2005

[25] Franz J, Baluja K L, Zhang R and Tennyson J 2008 *Nucl. Instr. Meths. Phys. Res. B* **266** 419–424

[26] Giusti-Suzor A and Lefebvre-Brion H 1977 *Astrophys. J.* **214** L104-103

[27] Giusti A 1980 *J. Phys. B: Atom. Molec. Phys.* **13** 3867-3894

[28] Gorfinkiel J D and Tennyson J 2004 *J. Phys. B: At. Mol. Opt. Phys.* **37** L343-350

[29] Gorfinkiel J D and Tennyson J 2005 *J. Phys. B: At. Mol. Opt. Phys.* **38** 1607–1622

[30] Green S 1981 *Ann. Rev. Phys. Chem.* **32** 103-138

[31] Giusti-Suzor A and Lefebvre-Brion H 1977 *Astrophys. J.* **214** 101–103

[32] Halmová G and Tennyson J 2008 *Phys. Rev. Lett.* **100** 213202

[33] Halmová G, Gorfinkiel J D and Tennyson J 2008 *J. Phys. B: At. Mol. Opt. Phys.* **41** 155201

[34] Hoffman K R, Dababneh M S, Hsieh Y, Kauppila W E, Pol V, Smart J H and Stein T S 1982 *Phys. Rev. A* **25** 1393–1403

[35] Jones M and Tennyson J 2010 *J. Phys. B: At. Mol. Opt. Phys.* **43** 045101

[36] Krauss M and Julienne P S 1973 *Astrophys. J.* **183** L139-141

[37] Lane N F 1980 *Rev. Mod. Phys.* **52** 29-119

[38] Lim A J, Rabadan I and Tennyson J 1999 *Mon. Not. R. Astro. Soc.* **306** 473-478

[39] Madden D and Tennyson J and Zhang R 2011 *J. Phys: Conf. Series* **300** 012017

[40] Mitchell J B A and McGowan J W 1978 *Astrophys. J.* **222** L77-79

[41] Morgan L A 1984 *Comput. Phys. Commun.* **31** 419-422

[42] Morgan L A and Gillan C J and Tennyson J and Chen X 1997 *J. Phys. B: At. Mol. Opt. Phys.* **30** 4087-4096

[43] Morgan L A, Tennyson J and Gillan C J *1998 Computer Phys. Comms.* **114** 120128

[44] Motapon O, Fifirig M, Florescu A, Waffeu-Tamo F O, Crumeyrolle O, Varin-Breant G, Bultel A, Vervisch P, Tennyson J and Schneider I F 2006 *Plasma Phys. Science Technology* **15** 23–32

[45] Mul P M, Mitchell J B A, D'Angelo V S, Defrance P and McGowan J W 1981 *J. Phys. B: At. Mol. Phys.* **14** 1353–1361

[46] Nestmann B M and Peyerimhoff S D 1990 *J. Phys. B: At. Mol. Opt. Phys.* **23** L773-L777

[47] Nestmann B M, Pfingst K and Peyerimfoff S D 1994 *J. Phys. B: At.Mol. Opt. Phys.* **27** 22972308

[48] Noble C J and Nesbet R K 1980 *Comput. Phys. Commun.* **33** 399-411

[49] Noble C J, Dörr M and Burke P G 1993 *J. Phys. B: At. Mol. Opt. Phys.* **26** 2983–3000

[50] Orel A E 1992 *Phys. Rev. A* **46** 1333

[51] Quigley L and Berrington K 1996 *J. Phys. B: At. Mol. Opt. Phys.* **29** 4529–4542

[52] Sanna N and Gianturco F A 1998 *Comput. Phys. Commun.* **114** 142-167

[53] Sarpal B K, Branchett S E, Tennyson J and Morgan L A 1991 *J. Phys. B: At. Mol. Opt. Phys.* **24** 3685–3699

[54] Sarpal B K, Tennyson J and Morgan L A 1994 *J. Phys. B: At. Mol. Opt. Phys.* **27** 5943–5953

[55] Schmidt M W and Ruedenberg K 1979 *J. Chem. Phys.* **71** 39513962

[56] Schneider A F and Rabadan I and Carata L and Andersen L H and Suzor-Weiner A and Tennyson J 2000 *J. Phys. B: At. Mol. Opt. Phys* **33** 4849-4861

[57] Schneider B I 1975 *Phys. Rev. A* **11** 19571962

[58] Schneider B I and Hay P J 1976 *Phys. Rev. A* **13** 20492056

[59] Schneider I F, Rabadán I, Carata L, Tennyson J, Andersen L H and Suzor-Weiner A 2000 *J. Phys. B: At. Mol. Opt. Phys.* **33** 4849–4861

[60] Shimamura I 1998 *Mol. Phys.* **93** 3-17

[61] Solomon P M and Klemperer W 1972 *Astrophys. J.* **178** 389-421

[62] Stibbe D T and Tennyson J 1996 *J. Phys. B: At. Mol. Opt. Phys.* **29** 4267–4283

[63] Stibbe D T and Tennyson J 1998 *Computer Phys. Comms.* **114** 236–242

[64] Szaboost and Lund 1996 *Modern quantum chemistry* Dover Publication, Inc

[65] Takagi H, Kosugi N and Le Dourneuf M 1991 *J. Phys. B: At. Mol. Phys.* **24** 711–732

[66] Tarana M and Tennyson J 2008 *J. Phys. B: At. Mol. Opt. Phys.* **41** 205204

[67] Tennyson J and Noble C J 1984 *Computer Phys. Comms.* **33** 421–424

[68] Tennyson J and Noble C J 1985 *J. Phys. B: At. Mol. Phys.* **18** 155–165

[69] Tennyson J 1988 *J. Phys. B: At. Mol. Opt. Phys.* **21** 805–816

[70] Tennyson J 1996 *At. Data Nucl. Data Tables* **64** 253–277

[71] Tennyson J 1996 J. *Phys. B: At. Mol. Opt. Phys.* **29** 18171828

[72] Tennyson J 2010 *Phys. Rep.* **491** 29–76

[73] Wigner E P 1946 *Phys. Rev.* **70** 606618

[74] Wigner E P and Eisenbud L 1947 *Phys. Rev.* **72** 29-41

[75] Zhang R, Baluja K L, Franz J and Tennyson J *J. Phys. B: At. Mol. Opt. Phys.*